J. Fluid Mech. (1977), vol. 81, part 3, pp. 465–495
Printed in Great Britain

Some experimental studies of vortex rings

By T. MAXWORTHY

Departments of Aerospace and Mechanical Engineering,
University of Southern California, Los Angeles

(Received 24 March 1976)

A series of experiments designed to reveal the properties of high Reynolds number vortex rings, using flow-visualization and laser-Doppler techniques, has uncovered several interesting and unexpected results. Starting at the beginning of the motion, at a nozzle, and proceeding downstream, these include the following.

(i) A formation process that is strongly Reynolds number dependent.

(ii) The amount of vorticity that appears downstream is very close to that predicted by a simple 'slug' model. However flow-visualization studies show that such a model is an oversimplification and that an excess of ring vorticity is probably cancelled by the ingestion of vorticity of opposite sign at the nozzle lip.

(iii) A new, bimodal form of vortex-core instability has been observed at moderate but not high Reynolds numbers.

(iv) Azimuthal inhomogeneities in the breaking of these, and the normal instability waves, create an 'axial' flow along the vortex core in the turbulent ring. This axial flow takes the form of a propagating wave that has many characteristics of a solitary wave. It is hypothesized that this axial flow prevents further ring instability.

(v) The long-term behaviour of the turbulent ring is marked by dramatic changes in its growth rate, which are probably related to changes in the 'organization' of the vortex core. The descriptive turbulent-ring model developed in Maxworthy (1974) is substantially confirmed by these experiments and by observation of ring propagation through a stratified ambient fluid.

1. Introduction and summary

The purpose of the present effort, at the beginning of the investigation, was to delineate the character of the well-defined 'turbulent'† vortex ring that ultimately emerges when a short pulse of fluid is ejected from an orifice at relatively large Reynolds numbers $\overline{U}_M D_M/\nu$.‡ Much apparently contradictory evidence had been published and it was our intention to try to bring some order to or, at least, identify a unifying concept for the subject. To do this, however, we found it necessary to study the whole sequence of events that occurs from the moment the ring is formed, by the 'rolling-up' of the vorticity produced by viscous forces at the orifice exit, to its ultimate decay many orifice diameters downstream. Here we present a number of experiments that attempt to elucidate the dynamical processes that are involved in the production of the final

† We put the word turbulent in inverted commas to emphasize the special character of this flow, which is quite different from our usual idea of a turbulent flow.

‡ $\overline{U}_M$ and D_M are the mean ejection velocity and orifice diameter and ν is the kinematic viscosity of the fluid.

state. A number of unexpected results have been found and these have led ultimately to an appreciation of the central role played by the formation process and how subtle changes in a variety of parameters can affect the problem. This has meant that for the evaluation of the results of other investigators critical pieces of information are often not reported and, in turn, that we have often had to guess, on the basis of the observed results and intuition, what the appropriate conditions were. As we proceed with the presentation of our new results we shall attempt to place them in perspective *vis-à-vis* these published results. Often this is not wholly satisfactory and points out some of the subtleties involved that had not been appreciated before.

Our experiments were performed at three different geographical locations, because a certain unique piece of apparatus existed at each one that could not be conveniently reassembled or manufactured in a common place. As a result coherent presentation of the results is difficult without the use of some unconventional techniques. The first of these is that, before presenting the detailed evidence, we describe the overall picture that has emerged. In this way we hope that the reader will be better prepared to digest the somewhat fragmented details that follow. The latter are grouped, also unconventionally, according to geographical location, each with its own subgroups: apparatus, results, etc.

In figures 1 (*a*)–(*f*), we show the sequence of events that determines the ultimate character of a vortex ring far from the location of its formation. We summarize all this information in as succinct a form as possible.

(i) Figure 1 (*a*) shows the formation process as inferred from measurements downstream and from observation of the motion of injected dye (see item (iv) below and § 2.2.3).

(ii) At $2{\cdot}5D_M$ from the nozzle we have found that: (*a*) the ring circulation Γ (figure 1 *b*) is approximately equal to that predicted by a simple 'slug' model, but that there is a weak Re dependence; (*b*) the vorticity distribution is highly peaked but weak vorticity exists all the way to the edge of the moving fluid volume; (*c*) the major diameter of the ring D depends strongly on the length of the ejected fluid slug L_M and only weakly on the Reynolds number $\overline{Re}_M$; (*d*) the minor diameter d depends strongly on $\overline{Re}_M$ and weakly on L_M (see item (iii) below); (*e*) the core, as defined in figure 5 (plate 2), contains only 50 % of the total vorticity in the ring (§ 2.2.1).

(iii) Approximately $5D_M$ downstream the core region develops an azimuthal waviness of wavelength λ (i.e. $\pi D/\lambda \equiv n$ waves can be counted). The ratio λ/d is approximately constant and hence λ or n becomes a measure of d at values of $\overline{Re}_M$ beyond the range of the system that measures d directly. n or $1/d$ increases monotonically with $\overline{Re}_M$, while the dependence on L_M is weak. A simple model is presented to explain this result (§§ 2.2.2 and 2.2.3 and the appendix).

(iv) The results in (ii) and (iii) imply that during the formation process (figure 1 *a*) the production of negative vorticity, i.e. opposite in sign to vorticity produced by flow separation at the lip, cancels part of the latter while the vortex rolls up in close proximity to the nozzle exit. This picture is confirmed by qualitative observations of dye motion and secondary vortex-ring formation.

(v) At approximately $10D_M$ the waves mentioned in (iii) have grown to finite amplitude and 'break' preferentially, i.e. the breaking does not occur at all azimuthal locations at the same time. This non-uniformity creates an azimuthal flow along the core that propagates as a wave motion (figure 1 *e*). This wave motion persists many diameters downstream and probably prevents further instability (§ 2.2.4).

(vi) The 'turbulent' ring thus formed, and measured at $14D_M$, consists of three distinct regions, ambient, outer-flow and core fluid (figure 1*e*), with well-defined interfaces between them. The core diameter d is larger and the circulation Γ is smaller than corresponding values upstream (at $2{\cdot}5D_M$). The ring growth rate α (figure 1*f*) is controlled by entrainment across the core/outer-flow interface and this is typically small (i.e. $\alpha = 6{\cdot}5\text{–}0{\cdot}5 \times 10^{-3}$). As the ring now propagates over long distances this growth rate undergoes dramatic changes as the 'organization'† of the core changes (§§2.2.4 and 3).

(vii) Observations of ring propagation through a stratified ambient fluid, in which case buoyancy forces destabilize the core/outer-flow interface and cause the ring to decrease in size, further confirm the picture presented in (vi) (and Maxworthy 1974). While experiments aimed at interfering with the axial flow show how important it is in maintaining a coherent, well-organized ring structure (§4).

2. Experiments at the Max Planck Institut für Strömungsforschung (M.P.I.S.), Göttingen

2.1. *Apparatus and instrumentation*

The equipment developed at M.P.I.S. by Dr Christian Liess and Dipl.Phys. Norbert Didden is built around two large glass-sided tanks containing water as the working medium (figure 2). The larger tank is 1 m square and 2 m long. In one end is located an interchangeable piston–cylinder–nozzle arrangement capable of producing vortex rings over a wide range of $\overline{Re}_M$. In the present experiments we used a 7 cm diameter nozzle coupled to a 15 cm diameter piston. The latter is driven by a cam/cam–follower system that is driven in turn by the output from a motor and a variable-speed gear-box through a magnetic clutch.

The lip of the nozzle is specially constructed to allow the injection of a small amount of dye into the core of the vortex ring. The ring history was then observed either by a camera traversing along a track at the same speed and parallel to the path of the ring or by a fixed camera with a lens of a long focal length, located some distance from the tank. Piston displacement–time records were obtained from a variable-reluctance displacement transducer whose output could be digitized and fed into a PDP 15 computer for analysis.

A second, smaller ($0{\cdot}4 \times 0{\cdot}4 \times 1$ m) tank is located within 2 m of the larger one and for our experiments was equipped with a 5 cm diameter nozzle driven by a 10 cm diameter piston. This piston is moved by the same cam/cam–follower arrangement as before through a long 3 mm diameter flexible stainless-steel cable that stretches over pulleys mounted in the ceiling of the laboratory.

This tank is equipped with a single-component laser-Doppler velocimeter (LDV) of a type originally developed at M.P.I.S. At its heart are two Wollaston prisms that at first produce two illuminating beams whose planes of polarization are at right angles. These two beams are brought to a focus in the middle of the tank and the light scattered from small particles in the water is collected by a lens. This light is then refocused through the second Wallaston prism onto the active elements of a double photodiode. This output is amplified, suitably filtered, and processed by a Thermo-Systems Inc.

† See §§2.2.4(*d*) and 5 for a detailed discussion of this concept.

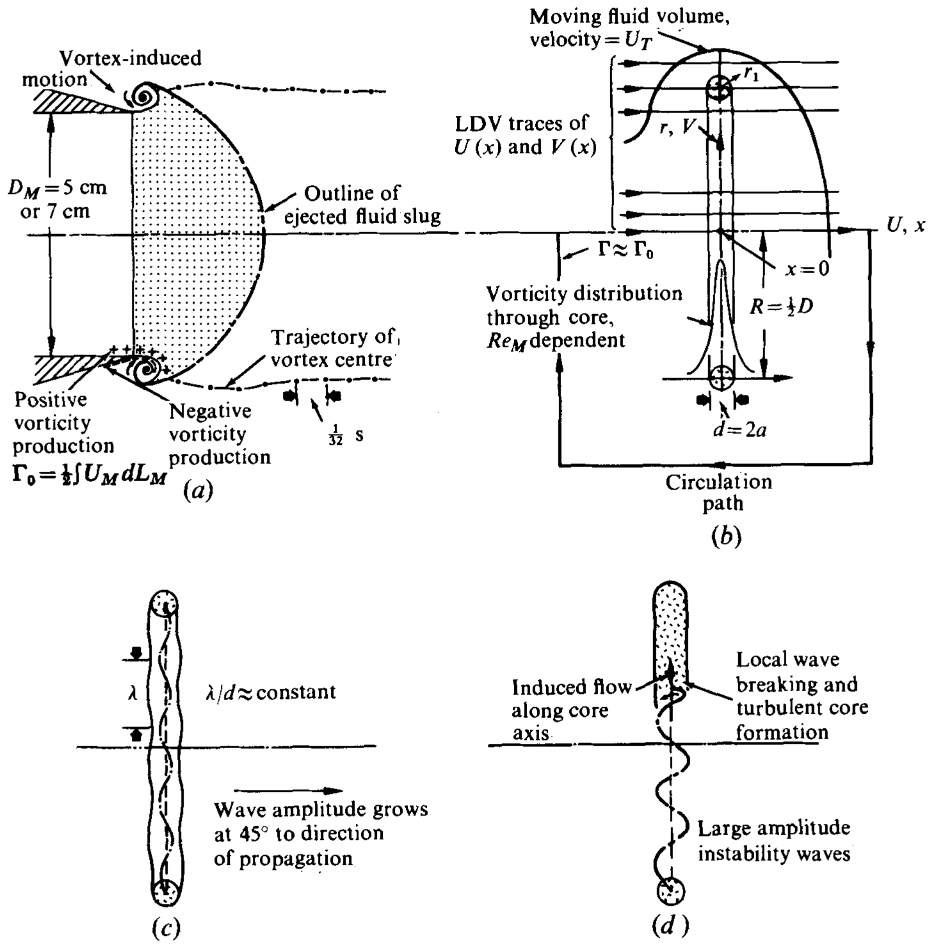

FIGURE 1. For legend see facing page.

Model 1501 tracking filter. An output voltage linearly proportional to the Doppler frequency, and hence to the velocity of particles passing through the focal volume, is then impressed on the vertical ordinate of either a Y–T recorder or an oscilloscope swept at a known rate. Thus the ultimate output is a velocity–time history that can be converted to a particle velocity–distance history by determining the velocity of the vortex ring as it passed through the focal volume.

The LDV optics are fixed in the laboratory frame. Velocity traverses can be obtained at various radii from the centre of the ring by moving the tank and nozzle up or down on a simple traversing mechanism. In a similar way, by moving the tank back and forth along its length, traverses at various distances from the plane of the nozzle can be taken. For the present experiments only two longitudinal stations were used, one $2{\cdot}5D_M$ from the nozzle, before instability occurred, and the other $14D_M$ downstream, after the instability had created a 'turbulent' vortex ring.

Both the U and the V velocity component could be measured independently and unambiguously by rotating the plane of the two beams through 90°.

These data could be used in various ways.

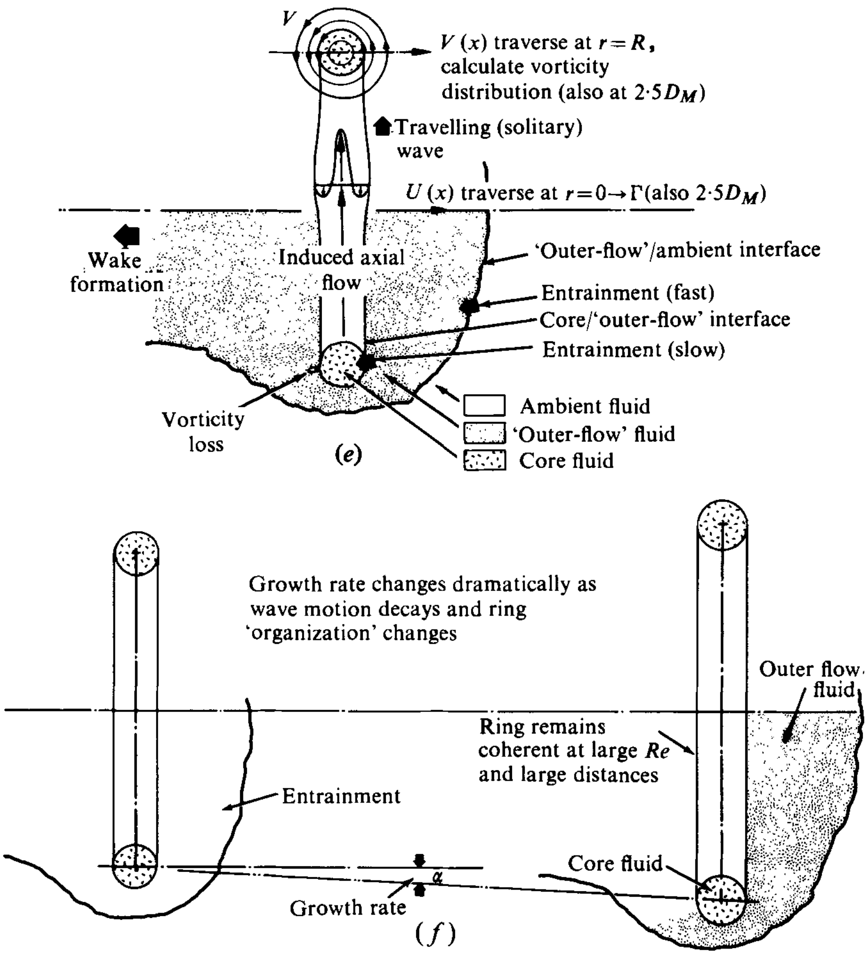

FIGURE 1. Composite diagram of vortex-ring history from its formation to its ultimate 'turbulent' states, summarizing the observations from all of the present experiments. (*a*) The inferred formation process, showing mainly production of negative vorticity by vortex-induced motions. (*b*) The first LDV station, at $2{\cdot}5D_M$, showing circulation loss and definitions of relevant parameters. (*c*) Start of core instability, at 5–$10D_M$, Re_M dependent. (*d*) 'Wave breaking' and the formation of a flow along the core axis, at 8–$15D_M$. (*e*) The second LDV station, at $14D_M$, showing the three major flow regions (core, outer flow and ambient fluid) and the interfaces between them, also the flow-inducing wave travelling around the vortex core. (*f*) Long-term growth of a 'turbulent ring' controlled by the slow entrainment across the core/outer-flow interface, over a distance of 15–$26D_M$ at M.P.I.S. and 15–$70D_M$ at Caltech.

(*a*) By measuring U as a function of x along the centre-line of the ring (i.e. $r = 0$) and integrating to find the area under the resulting curve, the total circulation of the ring Γ could be found (figure 1*b*).

(*b*) By measuring V as a function of x along $r = R$ (R being found from photographic data on dye injected into the core) and assuming that in the neighbourhood of the core the streamlines are circles (figure 1*e*), one can measure both the local circulation

$$\Gamma(r_1) = 2\pi r_1 V(r_1)$$

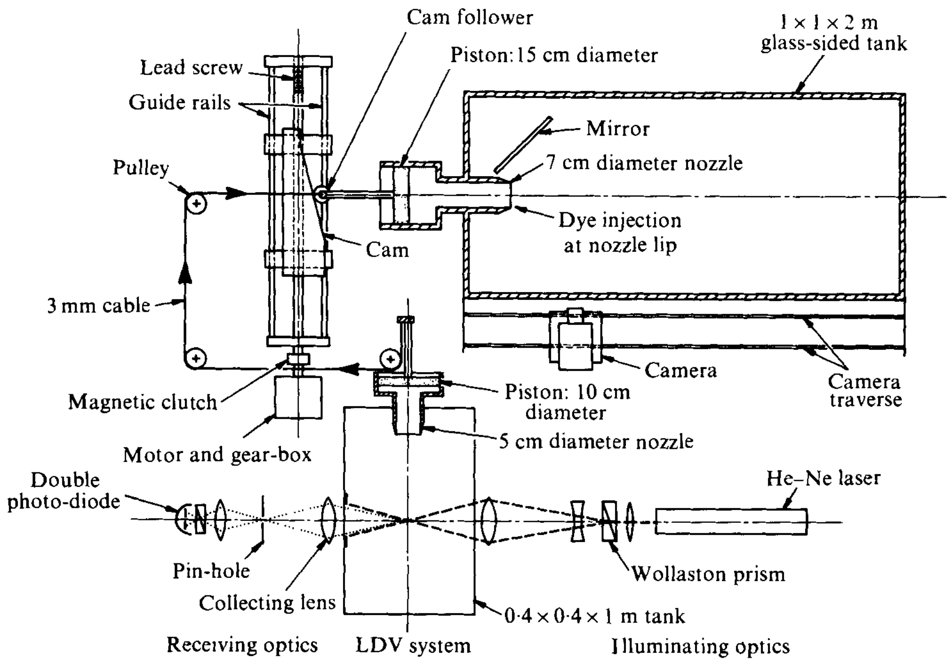

FIGURE 2. Apparatus at M.P.I.S., Göttingen.

and the vorticity distribution

$$\omega(r_1) = r_1^{-1}\, d[r_1\, V(r_1)]/dr_1.$$

(*c*) From $V(x)$ along $r = R$ one can find a convenient measure of the core diameter d. See figures 1 (*b*) and 5.

(*d*) From the maximum value of $U(x)$ taken at various radii one can find $U(r)$ in the x plane that includes the core centre ($x = 0$).

(*e*) From these data and the value of dV/dx at $x = 0$ one can calculate the vorticity precisely (mainly to check the accuracy of the assumptions made in (*b*)):

$$\omega = \partial V/\partial x - \partial U/\partial r.$$

The independent variables in this study were as follows.

(*f*) The nozzle diameter D_M and its shape (held fixed).

(*g*) The working fluid, in this case water at a known temperature and hence a known kinematic viscosity ν and known density ρ.

(*h*) The displacement L (or velocity), time t history of the ejected fluid. This is the hardest variable to quantify with precision since the shape of the L, t curve was somewhat variable as basic quantities such as the piston displacement and motor speed were changed. For the majority of the runs the piston velocity was constant over the middle 70 % of the total displacement with smooth acceleration and deceleration from and to zero. At the highest velocities in the large tank some overshoot in piston displacement took place but, as far as one can tell from gross observations, had little effect on vortex motion. Thus, assuming that the L, t curves are similar, two parameters were used to describe the motion. One, the length L_M of the ejected fluid slug, is simply the measured total piston displacement multiplied by the ratio of piston area to nozzle area. The second is the average ejection velocity $\overline{U}_M$, found by dividing the total piston displacement by the time that elapsed as the piston was being displaced from 5 % of its maximum velocity and back again, then multiplying, of course, by the piston/nozzle area ratio.

These quantities then define two dimensionless parameters:

$$L_M/D_M, \quad \overline{Re}_M = \overline{U}_M D_M/\nu.$$

2.2. *Results and discussion*

2.2.1. *The initial state at high* $\overline{Re}_M$. In this section we discuss, mainly, the results of LDV measurements at $2{\cdot}5D_M$ from the nozzle exit. At this location the path followed by the vortex centres is quite repeatable, to within $\pm\, 0{\cdot}5$ % of D in the radial direction; and the ring velocity U_T, as measured from x, t diagrams constructed from moving-picture sequences, is repeatable to within a maximum of $\pm\, 4$ %. The large variability was mainly due to a certain amount of looseness that developed in the mechanical piston-driving system, resulting in some non-repeatability in the piston displacement from run to run. Curiously this variability is not so noticeable in repeated LDV traces at the same location as it is in the moving-picture runs (the latter were performed approximately 14 days after the former and after the apparatus had been operated about four hundred times!). As a result the initial state under one set of operating parameters has been defined with reasonable precision and we have surveyed several others less completely.

(*a*) *Ring velocity and vorticity profiles.* In figure 3 (plate 2) we show U velocity traverses at various levels through the ring and in figure 4 the U velocity profile, at $x = 0$ (figure 1*b*), constructed from a series of such traverses. Deviations of the points from the 'average' curve gives some idea of the variability in the system since each point represents an average of five runs at each level, i.e. a total of 95 individual realizations. Under these circumstances the velocity peaks are hard to define unambiguously: in figure 4 the distance between the peaks is 1 cm. As a result it was decided to use a different approach that would give a total profile in only one experiment.

The LDV was rotated so as to measure the V velocity component and the focal volume set at the level $r = R$. It was then assumed that the streamlines were locally circular (figure 1*e*), leading to local measurements of $V(r_1)$, $\Gamma(r_1)$ and $\omega(r_1)$ (see § 2.1*b*). Figure 5 is a typical LDV output under these conditions and also shows how d was defined and measured. By graphically differentiating a smoothed tracing of this signal a graph of ω *vs.* r_1 was obtained (figure 6). Beyond $r_1 \approx 1$ cm, this method gave negative values of ω and was clearly inadequate. From $\partial U/\partial r$ and $\partial V/\partial x$, both at $x = 0$, it was possible to reconstruct the tail of this profile and show that over the inner $0{\cdot}5$ cm of the core the assumption of locally circular streamlines was a good one. Significantly, the vorticity distribution is monotonically decreasing all the way to the edge of the moving fluid volume, the latter being determined by photographing dye injected into the outer regions of the ring as it was being formed. The last calculated point has a vorticity which is more than two orders of magnitude smaller than the maximum value in the core but is still measurable, finite and positive. As postulated in Maxworthy (1972), it is this weak vorticity that diffuses across the boundary of the moving fluid volume, contaminates the outer irrotational fluid, causes it to be re-entrained and thus accounts for the growth of laminar vortex rings. Also shown in figure 6 are two curves

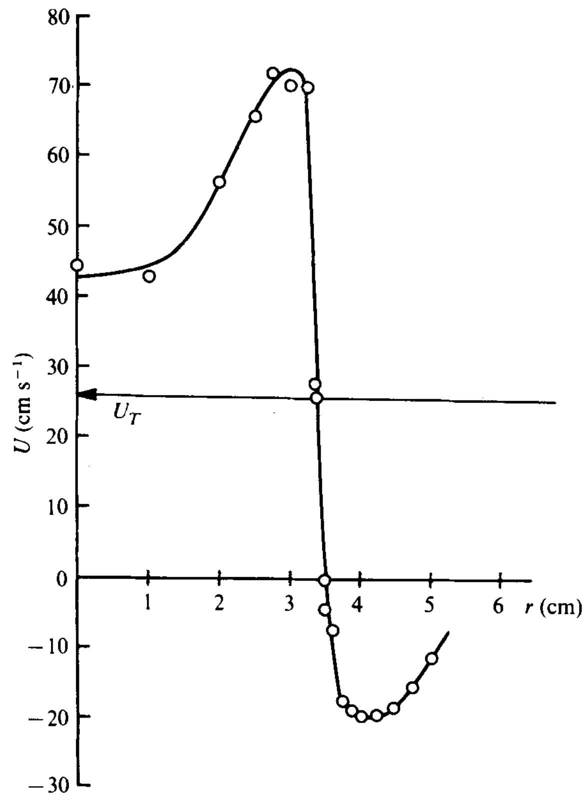

FIGURE 4. Velocity U *vs*. r in the x plane containing the vortex centres, i.e. $x = 0$ (figure 1*b*). Reconstructed from traverses like those shown in figure 3. Core diameter from $V(x)$ at $r = R$ is 0·77 cm, ring Reynolds number $U_T D/\nu = 1{\cdot}77 \times 10^4$, maximum vorticity $= 500\,\mathrm{s}^{-1}$.

that represent possible analytical descriptions of the measured curve. One, $(r_1^2 - a^2)^2$, is that used by Widnall, Bliss & Tsai (1974) in their calculation of the stability of the vorticity distribution. As can be seen it ignores the tail of the distribution, an effect that may be important in comparing the stability calculations with some of our later experiments (§2.2.3*e*). The final curve, $\mathrm{sech}^2 r_1$, typifies the exponential type of distribution that is probably a better description of the actual profile.

As a further indication of the importance of the tail of the distribution figure 7 compares the total circulation Γ with that contained within the core, i.e. $\Gamma_c = \pi d \hat{V}$, where $\hat{V}$ is the maximum value of V at $r_1 = \frac{1}{2}d$. We note that only about 50% of the total circulation is contained within the core. This comparison was suggested by the work of Sallet & Widmeyer (1974), who used Γ_c as a measure of the total circulation within the ring. As a result one must be careful when interpreting their results and conclusions and realize that Γ_c badly underestimates the quantity that is really of interest, namely Γ.

(*b*) *Ring diameter D as a function of the initial parameters.* In figure 8 we plot D/D_M *vs*. L_M/D_M over a wide range of $\overline{Re}_M$. Liess & Didden (1975) have performed experiments at values of $\overline{Re}_M$ as low as $\sim 10^3$ while ours cover the range up to $\overline{Re}_M \sim 7 \times 10^4$, and we note that the dependence on this parameter is very weak. Also included is one possible power-law dependence that fits the data reasonably well. We make use of this

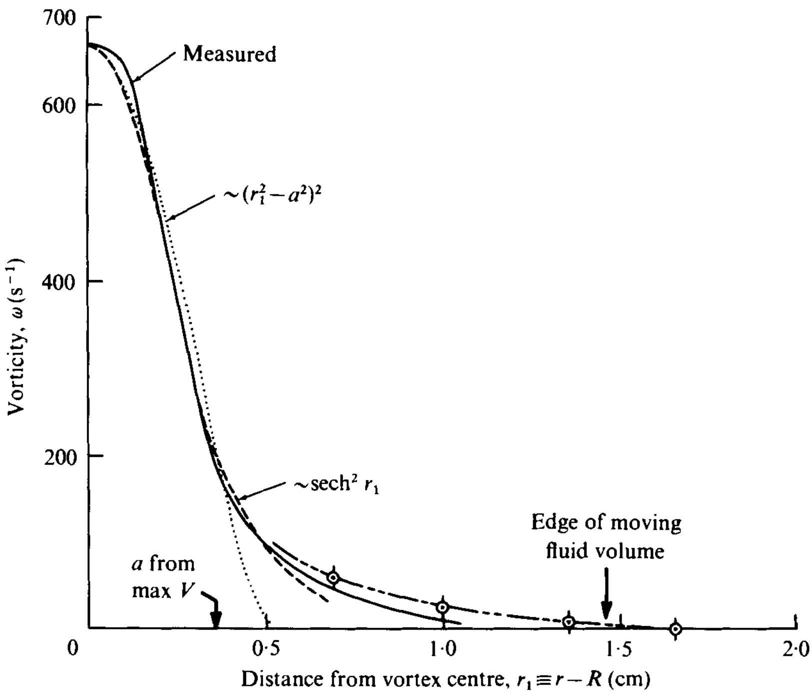

FIGURE 6. Measured vorticity distribution as a function of distance r_1 from vortex centre. ——, from $V(x)$ and assuming streamlines are locally circular; — · —, from complete expression for the vorticity $\partial V/\partial x - \partial U/\partial r$. Compared with expression used by Widnall *et al.* (1974) in their stability calculation and with an exponential distribution typified by sech^2 r_1. Ring Reynolds number $U_T D/\nu = 2{\cdot}1 \times 10^4$.

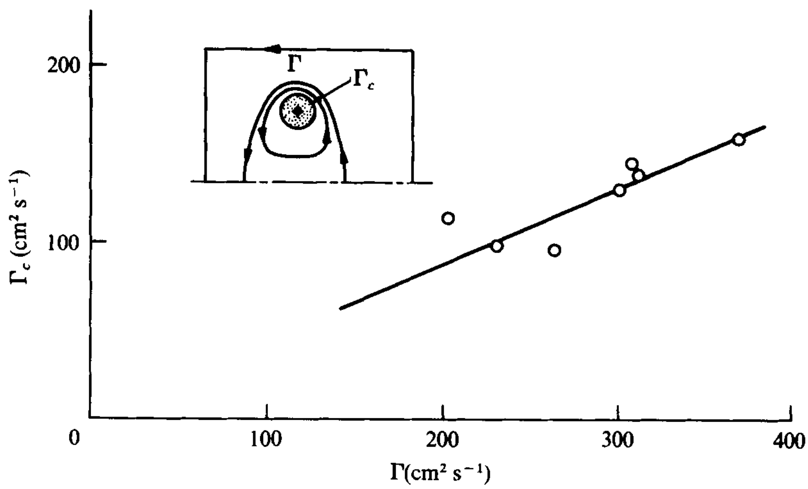

FIGURE 7. Core circulation Γ_c as a function of total circulation at $2{\cdot}5D_M$ downstream of nozzle; laminar case. For various L_M/D_M and $\overline{Re}_M$, with no discernible dependence on these two parameters.

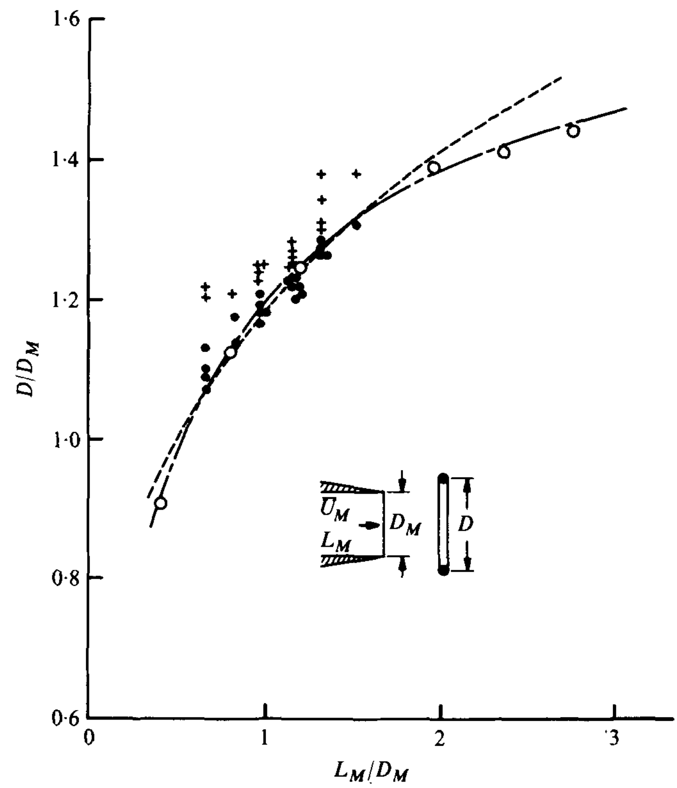

FIGURE 8. Ring diameter D/D_M at $2{\cdot}5D_M$ downstream *vs.* length of ejected fluid slug L_M/D_M. Over an $\overline{Re}_M$ range of approximately forty the ring diameter increases by no more than 10 % at fixed L_M/D_M. Present experiments: ●, $\overline{Re}_M \sim 2\times 10^4$; +, $\overline{Re}_M \sim 6\times 10^4$. ———, $D/D_M = 1{\cdot}18(L_M/D_M)^{\frac{1}{3}}$; ○, —·—, Liess & Didden (1975), $\overline{Re}_M < 10^4$.

later when we introduce a model that seems to be consistent with most of our observations.

(*c*) *Total circulation as a function of the initial parameters.* The data presented in figure 9 gives some clue to the nature of the ring formation process. One can calculate from the measured piston displacement curve and a simple 'slug' model the amount of vorticity that might have been formed at the nozzle exit. If we assume that the instantaneous nozzle exit velocity is U_M and that it is uniformly distributed over the exit cross-section, and if the increment of slug length is dL_M then the total initial circulation Γ_0 is

$$\frac{1}{2}\int_0^L U_M dL_M.\dagger$$

This is the simplest reference value that one can compute although it does not model the vortex roll-up process that occurs at the nozzle exit. Figure 9 shows that at $2{\cdot}5D_M$ from the nozzle apparently only a small amount of this circulation has disappeared, over a wide range of Γ_0, i.e. $\overline{Re}_M$, at fixed L_M/D_M. L_M/D_M becomes a factor only at large values, e.g. the experiment at a value of 2·4 is clearly different from the two closely

† Private communication with Dr V. Kulkarny (see Kulkarny 1977) and Dipl.Phys. N. Didden convinced me of the need for the factor $\frac{1}{2}$ which is not present in available, inviscid slug models (Linden & Turner, private communication; Saffman 1976).

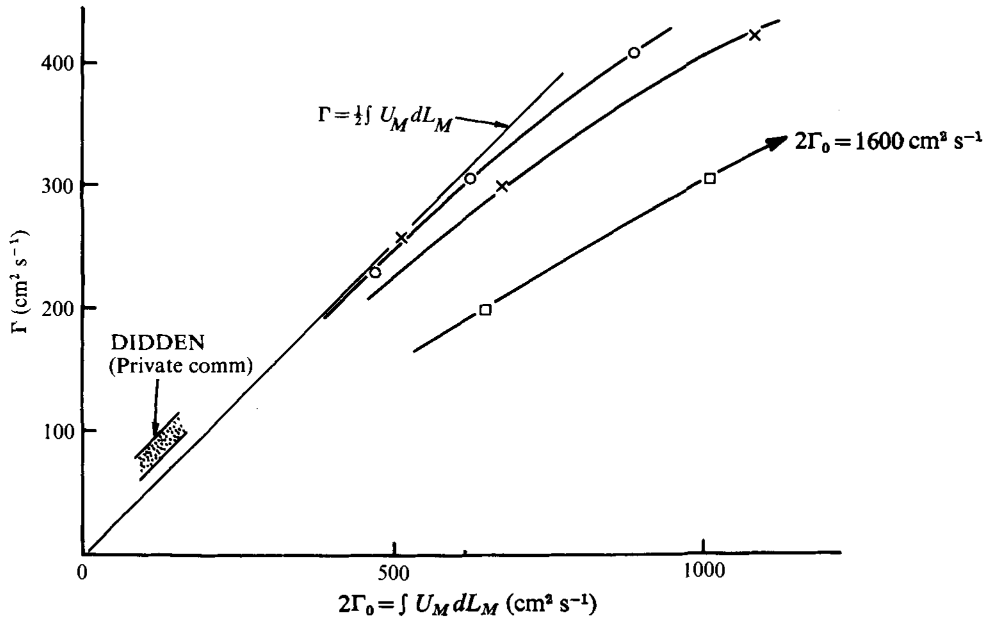

FIGURE 9. Measured circulation Γ at $2{\cdot}5D_M$ *vs.* reference circulation input at nozzle $2\Gamma_0 = \int U_M dL_M$ with L_M/D_M as the third parameter. The large loss in circulation can only have come from processes occurring at the nozzle and gives vital clues to the nature of the flow there. $\bigcirc$, $L_M/D_M = 1{\cdot}6$; $\times$, $L_M/D_M = 2$; $\square$, $L_M/D_M = 2{\cdot}4$.

spaced results at 1·6 and 2·0. This is almost certainly due to the formation of two vortices instead of one when L_M/D_M was large. The following vortex was weaker than the first and was not measured during the limited oscilloscope sweep duration that captured the first. We should note here that Dipl.Phys. N. Didden (private communication) found a result similar to this *before* the present measurements were undertaken. At lower Re_M [$\sim 3\times 10^3$] the circulation he measured was 130–160 % of $\frac{1}{2}\int U_M dL_M$, a result which, though compatible with the trend in figure 9, shows that the simple 'slug' model cannot be a good description of the formation process. These data indirectly tell us something about the ring formation process, a subject discussed in more detail § 2.2.3.

2.2.2. *Instability of the initial state.* (*a*) *Wavelength of instability compared with core diameter.* At a distance of 5–$8D_M$ from the nozzle (see § 2.2.2*c*) the fluid at the centre of the vorticity concentration becomes unstable. This instability has been previously described by Krutzsch (1939), Maxworthy (1972, 1974), Widnall & Sullivan (1973), Widnall *et al.* (1974) and Liess & Didden (1975, 1976), among others. It takes the form of an azimuthal waviness that grows in amplitude at 45° to the direction of propagation. It does not travel around the vortex core nor does it rotate in the rapidly swirling core flow. A plausible theoretical description has been given by Widnall *et al.* (1974), although, as we have already noted (§ 2.2.1*a*), the vorticity distribution used in their calculations ignores much of that in the real case. In our experiments we have carried measurements to much larger Reynolds numbers than before, and apart from a basic interest in the instability mechanism we should also like to use observations of the wavelength λ of the unstable waves diagnostically.

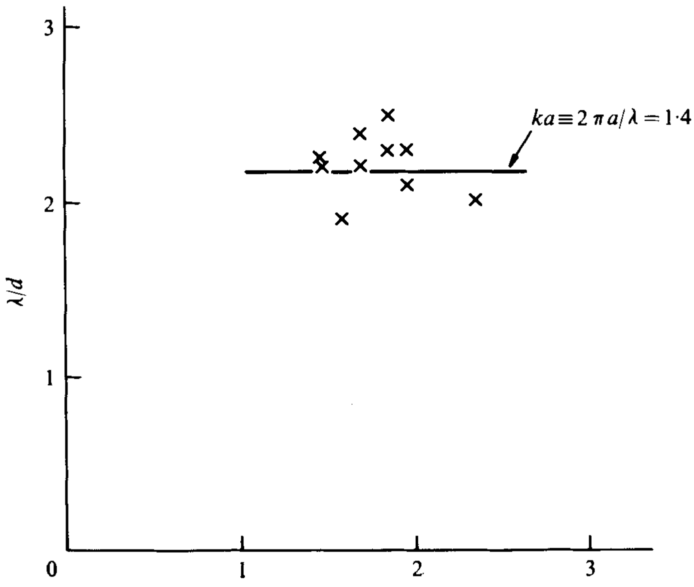

FIGURE 10. λ/d *vs.* $L_M D_M$ for a value of $\overline{Re}_M$ at the lower end of the available range. At higher $\overline{Re}_M$ existence of a bimodal form of instability made the unambiguous determination of λ impossible.

Since the present LDV system was not suitable for studying rings at very high $\overline{Re}_M$ we wished to establish a relationship between λ and d at low $\overline{Re}_M$ and then use λ as a measure of d at the higher values. The theoretical calculations previously mentioned show, in fact, that only a wave with a particular value of $Ka \equiv \pi d/\lambda$ can grow in the way observed, and our experiments have established that this is a plausible result. In figure 10 we show the evidence, gained at $\overline{Re}_M \sim 2{\cdot}7 \times 10^4$. [Because of the peculiarities of the instability process above this $\overline{Re}_M$, but below a value of $\sim 4{\cdot}5 \times 10^4$, λ could not be unambiguously defined in that range (see next subsection).] Despite the considerable scatter no clear trend appears and a value of $Ka \approx 1{\cdot}4$ is a reasonable description of the data.

(*b*) *Number of waves produced as a function of the initial parameters: implications for the core diameter d and the appearance of bimodal instability.* The data we are about to present are probably the most important discovered by this study and also the most controversial. Until recently two basic assumptions have been used in the description of vortex rings. The first was that the dimensionless group

$$\tilde{V} = U_T D/\Gamma \quad (= (2\pi)^{-1}[\ln(8D/d) - \tfrac{1}{4}])$$

in the Kelvin formula; Lamb 1932, p. 241) was a measure of the ratio d/D (e.g. Widnall *et al.* 1974). This point of view was denied by the experiments of Liess & Didden (1976),† who showed for L_M/D_M = constant and $2 \times 10^3 < \overline{Re}_M < 10^4$ that $U_T D/\Gamma$ and D/D_M were constant while the number of waves formed at instability increased from 5 to 11, i.e. that λ and hence d decreased by more than a factor of two over the

† I should also like to thank Dr C. Liess for private discussion on this point.

stated range of $\overline{Re}_M$. This was the first direct clue to the importance of $\overline{Re}_M$ in the description of vortex-ring structure and in what follows we add to this evidence. The second point of view evolved as the result of more than forty years of work on the inviscid roll-up of vortex sheets (e.g. Prandtl 1961; Betz 1932; Moore 1974) and suggested that at infinite $\overline{Re}_M$ the ring diameter D produced by such a rolling-up process would be $O(L_M)$,† with an infinitesimal core size d. Our present experiments have refined these views, and we ultimately introduce a new model that appears to contain elements of a correct description of the basic physical mechanisms involved.

Figure 11 is the crucial one. It shows how n (or $1/d$) varies with Reynolds number but is, unfortunately, confused by our uncertainty as to which value of the latter to use. The data of Liess & Didden (1976), and our extension of these to low $\overline{Re}_M$, were obtained with a piston displacement profile that gave a constant velocity over virtually the whole range. Hence the average jet velocity $\overline{U}_M$ and the maximum jet velocity $\hat{U}_M$ were the same. For our high velocity data $\hat{U}_M \approx 1{\cdot}35\overline{U}_M$ and the use of either value in constructing a Reynolds number is plausible. Up to this point the matter has not been critical because all of our previous data depended only weakly on $\overline{Re}_M$ and such subtle differences were not important; now we plot the data using both values in order to show how the results and their interpretation are affected.

Several interesting points should be noted. First, n increases monotonically with $\overline{Re}_M$, with no indication that the curve is levelling out. Second, as L_M/D_M is increased by 50 %, n decreases slightly, i.e. the functional dependence on L_M/D_M is very weak but noticeable. Third, if we wished to describe the result by a power law $n = \kappa\, Re_M^m$ then $\frac{1}{4} < m < \frac{1}{2}$. Under the present circumstances it seems unwise to try to be more accurate in this assessment, but $n = \kappa_1 Re_M^{\frac{1}{2}}$ certainly overestimates the upper curve while $n = \kappa_2 Re_M^{\frac{1}{4}}$ underestimates the lower. The curve ($\sim Re^{0{\cdot}4}$) shown on figure 11 (*b*) represents an average over all the experimental points and will prove useful as a reference in the discussion below (§ 2.2.3).

The detailed results in the range $2{\cdot}5 \times 10^4 < Re_M < 5{\cdot}0 \times 10^4$ have been omitted to avoid confusing figure 11 more than is necessary and are presented separately in figure 12. The main point to note here is that a new type of instability appears. Photographs are shown in figure 13 (plate 3), in which waves of two wavelengths are seen to exist on the core at the same time. Moving-picture sequences show that the smaller wavelength appears first but that alternate waves are displaced to become the peaks of a wave with wavelength twice the original. The details do not repeat from run to run and sometimes the shorter waves do not appear at all at low $\overline{Re}_M$. As $\overline{Re}_M$ increases the shorter waves dominate and eventually the wavelength doubling process ceases.

Without further work the precise reason for the appearance of this new instability is not clear. However, one can speculate that it must be tied to the form of the vorticity profile we have measured. The initial instability responds on a scale appropriate to the width of the very peaked vorticity distribution (i.e. the short wavelength); however, as it grows in amplitude, the wings of the distribution become more important, the apparent length scale increases and the waves respond by increasing their wavelength. As $\overline{Re}_M$ increases the distribution becomes so peaked and the wings so weak that the production of the longer wave does not have time to occur before the waves 'break' and the ring becomes 'turbulent'.

† Prof. P. G. Saffmann, private communication.

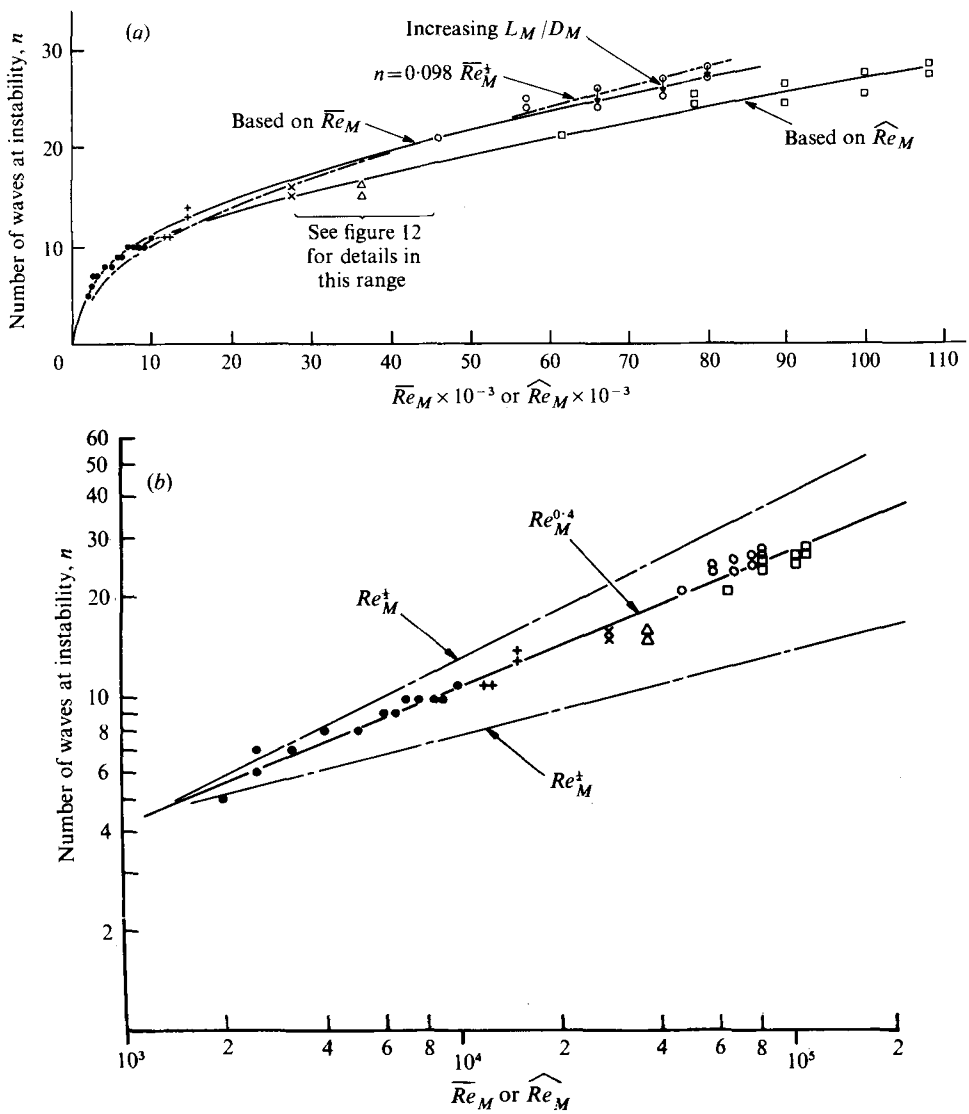

FIGURE 11. (*a*) Number of waves at instability n *vs.* a Reynolds number based on either $\overline{U}_M$ or the maximum jet velocity $\hat{U}_M$. Present experiments: +, $L_M/D_M = 1{\cdot}5$; 7 cm nozzle, large tank; ○, □, $L_M/D_M \leqslant 1{\cdot}5$, 7 cm nozzle, large tank; △, ×, 5 cm nozzle, small tank. ●, Liess & Didden (1976), $L_M/D_M = 1{\cdot}4$. (*b*) Same as (*a*) but with logarithmic ordinate and abscissae.

(*c*) *Start and duration of instability.* To complete the discussion on the instability process we show in figure 14 the distance from the nozzle at which waves were first visible (X_w/D_M) and the distance at which they broke to create a turbulent ring (X_U/D_M). Clearly both of these are subjective judgements of the observer and are mainly given to indicate how rapidly the waves grow and break at high $\overline{Re}_M$ compared with the more casual tendency shown in the data of Liess & Didden (1975) at low $\overline{Re}_M$.

2.2.3. *The implied nature of the ring formation process.* It is evident that a unique distribution of ring vorticity must be produced by a given piston motion and nozzle

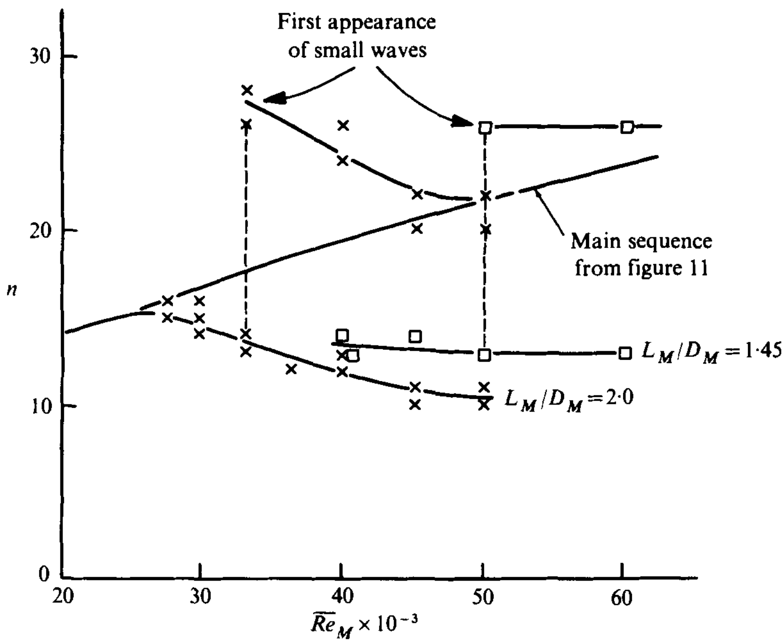

FIGURE 12. Same as figure 11 (*a*), but showing details of the formation of a bimodal form of instability at intermediate $\overline{Re}_M$.

geometry. To date, direct observation of the processes which produce this distribution have been restricted to flow-visualization studies and these have given no quantitative information. In the present work we have extended such visual studies to higher Reynolds numbers than before but, more critically, have taken quantitative data on the vorticity distribution itself, the total circulation and the core size produced under certain circumstances. Unfortunately most of this information was gathered several nozzle diameters downstream of the region of formation and hence some details on formation tend to be masked, to some extent, by processes which modify the results between the two locations.

As a summary of the flow-visualization studies we show, in figure 1 (*a*), an actual tracing of the location of the vortex centre during the formation process and the rolled-up region of dyed fluid that has originated at the lip and serves to mark the ring vorticity in a crude way. The picture is drawn at the instant the outflow from the nozzle has ceased. Note that during formation the core region stays in close proximity to the nozzle lip. Moving-picture frames taken before the one drawn here show the core centre moving away from the lip, as more and more vorticity-containing fluid is rolled up into the core, until it reaches the position shown. Thereafter the core centre moves along the trajectory shown in figure 1 (*a*). It is quite evident that an intense, vortex-induced flow is produced at the *outer edge* of the lip and that this must create vorticity of opposite sign (negative) to that produced by the main jet flow (positive). One other piece of secondary evidence strengthens this position. In figuie 15 (*a*) (and figure 16, plate 4) we show how a secondary vortex of negative sign is formed within the nozzle and propagates backwards into the nozzle. Its own motion creates more positive vorticity, which is ingested into this ring and eventually destroys it. In

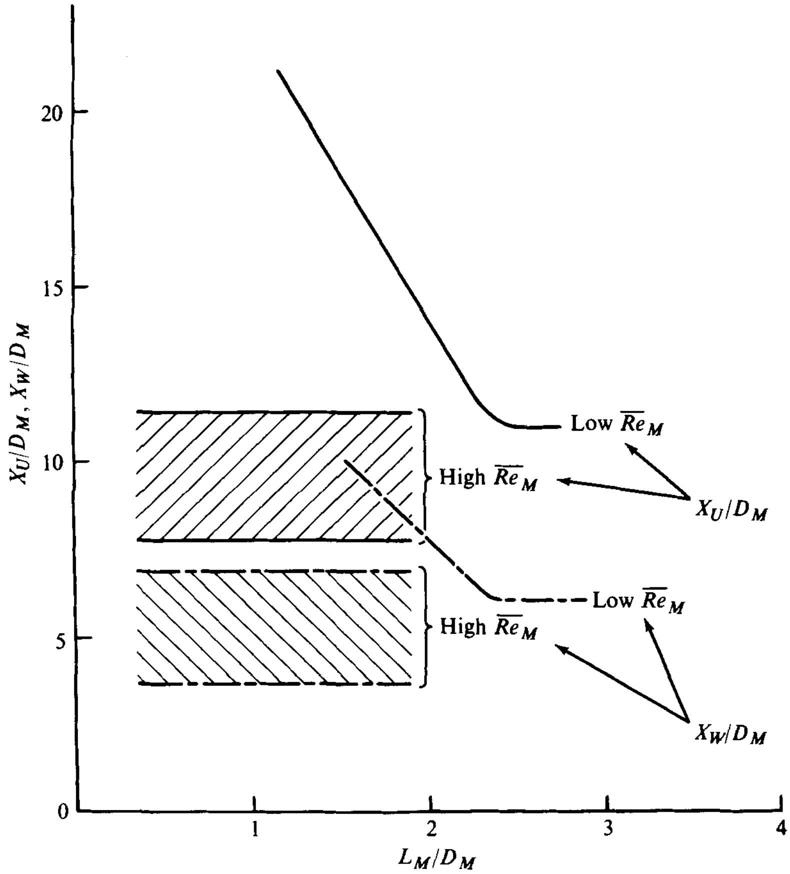

FIGURE 14. Location of start of ring instability (X_W/D_M) and of wave breaking and 'turbulent' ring formation (X_U/D_M) *vs.* L_M/D_M. Compared with data at low $\overline{Re}_M$ from Leiss & Didden (1975). No discernible trend with this parameter was noted in the present experiments so all data are included in the shaded regions.

figure 15(*b*) we show the same situation for an orifice plate; in this case the secondary vortex moves away from the solid surface and is not destroyed. Observations of such secondary vortices are common among experimenters who use this geometry! The primary ring is far enough away from the nozzle that, at this stage, it does not ingest any of the negative vorticity. However the kinetic energy in the secondary vortex represents a drain on that in the primary and must account for some small loss initially.

We find that at the Reynolds numbers of interest in the present work the total amount of vorticity found downstream (i.e. the circulation) is very close to that predicted by a 'slug' model. In view of the flow-visualization results it is clear that much more positive vorticity must be produced than is predicted by this model but that most of the excess is cancelled by negative vorticity production. At very low $\overline{Re}_M$ N. Didden (private communication) has found that the velocity field created by the rolling-up of the vortex creates much more total vorticity than the model would suggest while the trend at high $\overline{Re}_M$ (i.e. figure 9) shows less production. Thus the balance between positive and negative production clearly depends on $\overline{Re}_M$ in a weak

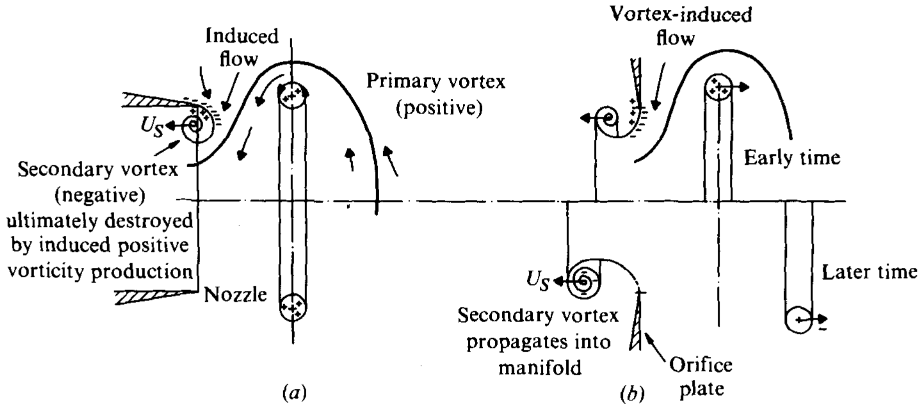

FIGURE 15. (*a*) As the vortex ring moves away from the nozzle the flow it induces creates a secondary vortex of vorticity of opposite sign that propagates back into the nozzle and is destroyed. (*b*) Similar observation for a thin orifice plate; but now as the secondary vortex moves away from the hole positive vorticity production ceases and the ring is not destroyed.

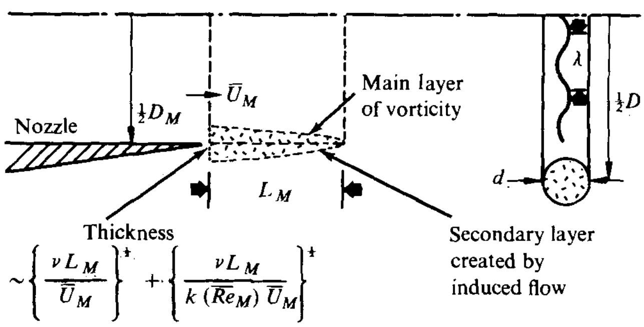

FIGURE 17. Diagrammatic sketch of ring formation model in which only vortical fluid rolls up to form a vortex core. Although the boundary layers are shown stretched out they actually start to roll up immediately they exit from the nozzle.

way, but exactly how the balance is struck is unclear without further detailed measurements at the nozzle lip itself.

Not only is the total amount of vorticity of interest but also the size of the region within which it is contained. Figure 6 suggests that the core diameter as defined in figure 5 is a reasonable measure of the extent of this region, while figure 11 (*b*) shows the size to be Reynolds number dependent. A simple viscous diffusion argument, as suggested by Moore & Saffman (1973), shows that the dependence should be as $\overline{Re}_M^{-\frac{1}{2}}$, but this clearly overestimates the experimental result. A simple model (see appendix and figure 17) which assumes that the fluid that rolls up to form the core is that which has gained vorticity from viscous processes at the lip predicts, in its simplest form, that $d \sim \overline{Re}_M^{-\frac{1}{4}}$ (although various modifications could increase the exponent to a value of around $-0{\cdot}3$). This result clearly underestimates the experimental trend but the validity of the assumptions on which it is based cannot be rejected yet because the measurements were made at least $5D_M$ downstream and must contain an element due to the diffusion of the initial vorticity distribution during the time the ring propagates and before it becomes unstable. As a result one would expect the exponent to be increased above the value quoted previously. The model is also consistent with the inviscid limit, in which d, as defined, is equal to zero at infinite $\overline{Re}_M$.

Thus this model, which depends directly on the volume of vortical fluid created initially, is not inconsistent with our other results but needs to be investigated in more detail before all the processes can be said to be fully understood.

2.2.4. *Formation and properties of 'turbulent' rings.* (*a*) *Breaking of instability waves, formation of axial flow and solitary wave, solitary wave-speed.* As we have already mentioned, and as has been observed by many other investigators, when the instability waves reach a finite amplitude they 'break' to form a 'turbulent' ring. The details of this process are quite fascinating and we show a photograph in figure 18 (plate 5) and a sketch in figure 1 (*d*). Before breaking the waves grow at 45° to the direction of ring propagation and neither propagate nor rotate. As suggested by Widnall *et al.* (1974), this is probably because the radial mode number and 'axial' wavenumber have exactly the right values to induce a velocity field that prevents rotation. However, at large amplitudes such a balance is no longer possible, and the waves begin to rotate while the core fluid mixes and becomes 'turbulent'. At the high $\overline{Re}_M$ of interest here the breaking does not take place uniformly around the core and the azimuthal pressure gradients associated with this non-uniformity create a *local* azimuthal flow (i.e. a flow along the axis of the vortex core, called an 'axial' flow in this paper) as shown diagrammatically in figure 1 (*e*). In the movie sequences that are a continuation of those shown in figure 18, for example, this axial flow can be clearly seen as a pulsation in the core diameter and a motion of the non-uniformly distributed dye. The point is not shown well by 'stills' taken from these movies and so a different technique was used for presentation here. In figure 19 (plate 6), we show the motion of dye initially introduced at only two locations on the top and bottom of the nozzle. These dye spots are seen to move around the core intermittently as the wave of axial flow travels around the core. By timing these pulses in several cases, we have determined wave speeds that are very close to the maximum swirl velocity in the cores. Thus by using available information about waves propagating in vortex cores (e.g. Leibovich & Randall 1972) it is clear that only one wave is propagating around the core and that it is probably a wave of expansion, i.e. the central part of the induced axial flow is in the direction of propagation. We also note a reversed axial flow at larger radii since the total 'axial' momentum must be zero. In view of the fact that there is only one wave and that the maximum 'axial' flow velocity is large (of order one-half of the wave speed) we suggest that this wave is most probably a finite amplitude, solitary wave. We believe that this axial flow has a profound effect on the properties of the vortex core in that it prevents further ring instability. As we shall show, the turbulent core that has been formed has a vorticity distribution that could be unstable by the criteria devised by, for example, Widnall *et al.* (1974). However Yuen (1973) has shown that for long waves, at least, axial core flow reduces the growth rate of unstable disturbances while Moore & Saffman (1975) have suggested the possibility that axial flow also stabilizes the short wavelength instability of the type that we observe. In the time it takes for the wave to propagate around the core any instability can grow to only very small amplitude before it is destroyed by the wave-induced axial flow. One result is that the core remains coherent for a long time and grows only very slowly. At low $\overline{Re}_M$ ($\sim O(10^4)$) the wave breaking process is much more uniform (figure 16 (*b*), plate 4)

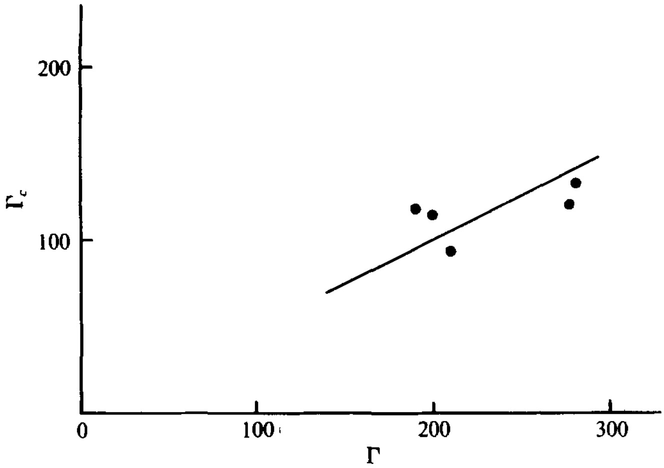

FIGURE 21. Amount of circulation Γ_c contained within the core compared with total circulation Γ for turbulent ring at $14D_M$. Cf. figure 7.

and the axial flow, if one exists, is very weak. The core structure breaks down much more rapidly and the ring grows much faster than at high $\overline{Re}_M$, possibly because some form of core instability now can exist, although its exact nature is not shown clearly by the present work (see also §5).

(*b*) *Structure of the turbulent core.* LDV measurements at $14D_M$ from the nozzle were much harder to perform than those at the first station, mainly because the path followed by each ring varied considerably from run to run. Often the core region would miss the LDV focal volume completely and only a few suitable V velocity traverses were obtained in each case. A sample is shown in figure 20 (plate 7). The difference between these traces and those for the laminar state (i.e. figure 5, plate 2) is quite evident. Whereas the latter is smooth with a gently rounded peak the former show evidence of strong velocity discontinuities and the transition at the peak is very abrupt. Such a rapid transition argues strongly for the type of interface that we have observed in dye studies (e.g. Maxworthy 1974; and §3.2 below), the mean azimuthal vorticity being large on one side (the core) and low on the other (the 'outer flow' of figure 1*e*). Unfortunately, we have not been able to relate this velocity transition to the dye transition unambiguously and can only suggest that they are probably the same. In the core the large mean vorticity suppresses turbulent fluctuations perpendicular to the vortex lines, so that only azimuthal fluctuations are large and seem to consist mainly of the wave motion that we have previously discussed. In the outer flow the mean azimuthal vorticity is low (but it still accounts for a considerable fraction of the total circulation; figure 21 shows that, as in the laminar case, the core still accounts for only 50 % of the total circulation). As a result the turbulence in the outer flow is of a more conventional, three-dimensional character and in particular the interface between it and the ambient fluid is very contorted and entrains ambient fluid very rapidly (as in a thermal, for example). However the overall growth of the system is controlled, as in many processes that involve several different rates, by the slowest entrainment, that at the core/outer-flow interface, because there the turbulent fluctuations are suppressed by the mean vorticity. Thus this interface takes on a central

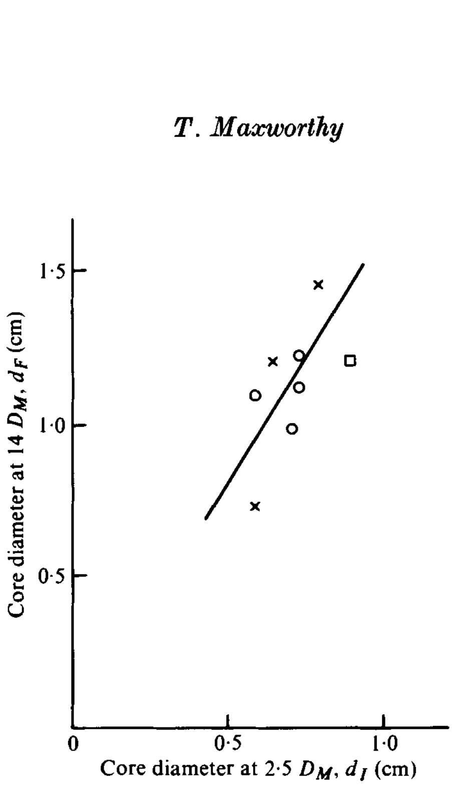

FIGURE 22. Change in core diameter d from $2{\cdot}5D_M$ to $14D_M$, showing the increase due to the instability and wave breaking processes.

role since it must simultaneously entrain outer-flow fluid and also feed the outer flow with the vorticity it needs to remain turbulent. Exactly how the interface performs this task is not completely clear, but since the vorticity gradients are large diffusion must play a role. Diffusion is also enhanced by the propagating solitary wave, which alternately sharpens and broadens the vorticity gradient as it passes a particular point on the core, and by the effect of the outer-flow turbulent fluctuations. We have also observed the direct removal of core fluid by the turbulent outer flow (as shown in figure 1 *e*) but this process seems to become less important once the core is established and the ring travels over long distances. The excess fluid entrained across the outer-flow/ambient-fluid interface that is not needed to account for the overall growth of the moving volume is then rejected into a wake, carrying with it a small amount of mean vorticity. This process is quite clearly shown in Maxworthy (1974) and the experiments to be reported in § 3.

(*c*) *Changes in core diameter and ring circulation during instability.* In figures 22 and 23 we relate the circulation and core diameter at $2{\cdot}5D_M$ to those at $14D_M$ and show that the former increases by about 50 % through the instability process while approximately 16 % of the initial circulation is lost.

(*d*) *Growth history of turbulent rings.* We now present some evidence that helps support the statement that the core entrainment rate is very low and must control the overall growth of the ring. In Maxworthy (1974) we measured growth rates $O(10^{-2})$ and were left with the feeling that this might be a universal result for all 'well-organized' vortex rings. The present experiments, which often show a growth one order of magnitude smaller than this, indicate that this is not so and that more subtle processes are at work than were at first realized. In figure 24 we show a truly typical result for a high $\overline{Re}_M$ ring in the large tank. Characteristically, the ring diameter at first over-

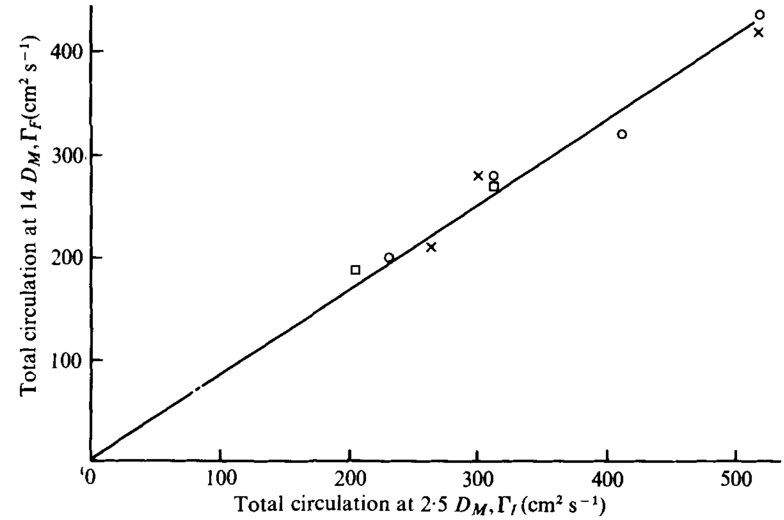

Figure 23. Change $\Delta\Gamma$ in total circulation, showing the small decrease induced by instability and wave breaking: $\Delta\Gamma/\Gamma_I \sim 16\%$.

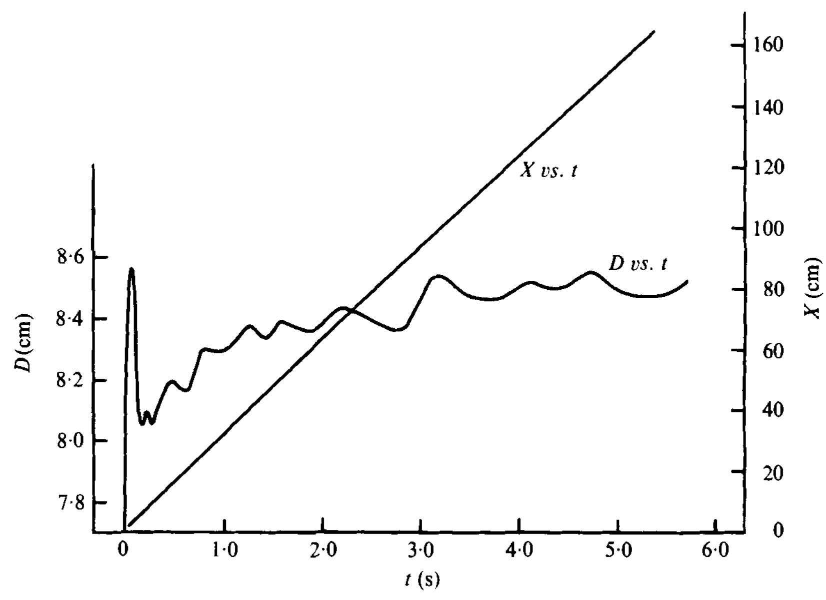

Figure 24. Growth in ring diameter D and ring displacement X *vs.* time t. $U_{\text{init}} = 31{\cdot}5\ \text{cm s}^{-1}$, $Re = 25{\cdot}8 \times 10^3$, $\bar{\alpha} = 0{\cdot}001$, $\overline{Re}_M = 7{\cdot}3 \times 10^4$, $L_M/D_M = 0{\cdot}98$, $D/D_M \approx 1{\cdot}18$.

shoots its equilibrium level (cf. figure 1*a*) and then oscillates† as it travels down the tank. One can readily measure the initial ring Reynolds number ($Re = U_{\text{init}}D/\nu$) and, by drawing a mean line through the oscillating curve for D, the overall growth rate α. Values for series of experiments are shown in table 1, with Re typically one-third of $\overline{Re}_M$ and with $6{\cdot}5 \times 10^{-3} > \alpha > 0{\cdot}5 \times 10^{-3}$. No clear trend in the growth data is evident:

† This is not necessarily an oscillation of the diameter D, but often changes in the shape of the ring are involved also.

Experiment	L_M/D_M	$\overline{Re}_M$	Re_{init}	α
F 4–2	1·18	$7·9 \times 10^4$	$2·6 \times 10^4$	$1·8 \times 10^{-3}$
4–3	1·18	$7·9 \times 10^4$	$2·6 \times 10^4$	5×10^{-3}
4–4	0·98	$7·9 \times 10^4$	$2·6 \times 10^4$	$1·5 \times 10^{-3}$
4–5	1·31	$6·6 \times 10^4$	$2·5 \times 10^4$	$3·2 \times 10^{-3}$
4–6	1·18	$6·6 \times 10^4$	$2·4 \times 10^4$	$1·2 \times 10^{-3}$
4–7	0·98	$6·6 \times 10^4$	$2·5 \times 10^4$	$2·6 \times 10^{-3}$
4–8	0·66	$6·6 \times 10^4$	$2·1 \times 10^4$	$3·7 \times 10^{-3}$
4–9	1·31	$4·5 \times 10^4$	$1·8 \times 10^4$	$6·5 \times 10^{-3}$
5–1	1·31	$5·7 \times 10^4$	$2·2 \times 10^4$	$3·4 \times 10^{-3}$
5–2	1·18	$5·7 \times 10^4$	$2·14 \times 10^4$	$0·9 \times 10^{-3}$
5–3	0·98	$5·7 \times 10^4$	$2·2 \times 10^4$	$1·4 \times 10^{-3}$
5–4	0·82	$5·7 \times 10^4$	$2·1 \times 10^4$	$0·7 \times 10^{-3}$
5–5	0·66	$5·7 \times 10^4$	$1·9 \times 10^4$	$1·9 \times 10^{-3}$
5–6	0·66	$5·7 \times 10^4$	$2·0 \times 10^4$	$1·7 \times 10^{-3}$
5–7	1·31	$7·3 \times 10^4$	$2·7 \times 10^4$	$3·3 \times 10^{-3}$
5–8	1·18	$7·3 \times 10^4$	$2·8 \times 10^4$	Undefinable
5–10	0·98	$7·3 \times 10^4$	$2·6 \times 10^4$	$0·5 \times 10^{-3}$
5–11	0·82	$7·3 \times 10^4$	$2·6 \times 10^4$	Undefinable
5–12	0·66	$7·3 \times 10^4$	$2·4 \times 10^4$	$0·5 \times 10^{-3}$
5–13	1·51	$7·9 \times 10^4$	$3·0 \times 10^4$	5×10^{-3}

TABLE 1†

in all cases the cores appeared to be well organized with no clear indication of any major differences between them to account for the large differences in growth rate. However at lower $\overline{Re}_M$, e.g. the ring shown in figure 16 (*b*), the cores are fat, there is little axial flow, and the growth rates are considerably larger (typically 15×10^{-3}). This result and those which follow (§3) suggest the importance of a concept which, although hard to define quantitatively (see §5), can be useful for describing results such as these. The concept is the one that relates to the 'organization' of the vortex core. Clearly the small α, high $\overline{Re}_M$, compact cores are 'well organized', while the fat, low $\overline{Re}_M$, large α cores are 'disorganized'. The difference somehow depends on the vorticity distribution (i.e. whether it is peaked or broad) and the existence of a travelling axial wave. We shall comment further on these ideas in §5.

3. Experiments at the California Institute of Technology, Pasadena

3.1. *Introduction*

In Maxworthy (1974) we showed that, at moderate Reynolds numbers and over a propagation distance of about $35D_M$, the growth of a turbulent ring was a linear function of distance. Later it came to our attention that Arnold (1974) had discovered a deviation from this linear growth as a ring propagated over longer distances. In his experiments a ring was ejected against the flow of a water stream in a long flume. This enabled him to observe the ring for a much longer time than was available in a stationary fluid in the same tank. His results invariably showed that the growth rate increased after an initial linear portion. This effect was enhanced by placing

† I wish to thank Cand.Phs. H. H. Claus for reducing the photographic data and producing curves from which this table was prepared.

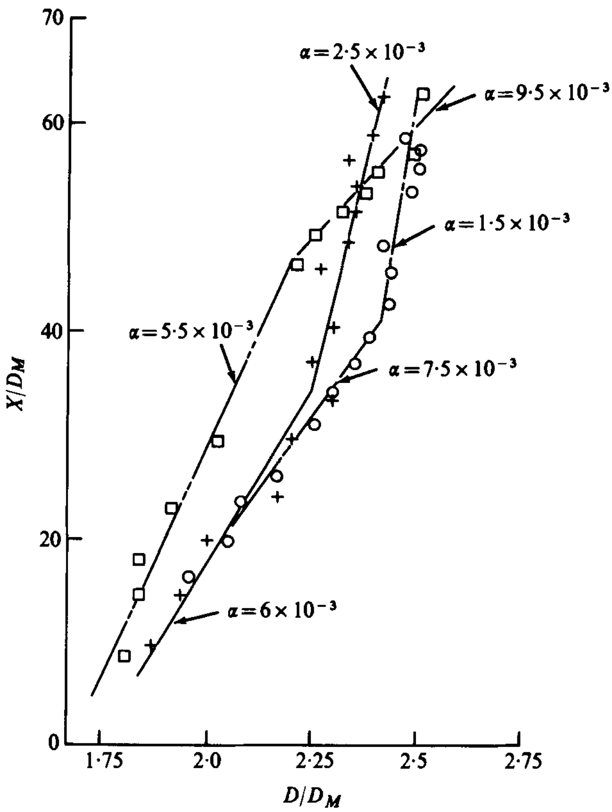

FIGURE 25. D *vs.* X curves from Caltech tank showing at least two types of transition that dramatically change the growth rate of the turbulent ring. $Re_{init} = 2 \times 10^4$, no close control of L_M/D_M, $D_M = 7{\cdot}6$ cm.

turbulence-producing grids in the flow upstream of the average location of the ring. Since, even when there were no grids, the flume flow must have been turbulent the question was raised as to whether or not this was the mechanism causing the difference between our results. We therefore decided to look at ring propagation in a very long tank of stationary (hopefully) non-turbulent fluid. The only available tank was located at Caltech and we performed a set of experiments there.

3.2. *Apparatus and procedure*

The water tank, located in the Keck Laboratory at Caltech, is 1 m square and 5·5 m long. In this we placed a vortex generator that was a slight modification of that used in Maxworthy (1974). The ring was produced by a sharp-edged orifice plate with an exit diameter of 7·6 cm located in the centre of the 1 m square cross-section of the tank. A ring was produced by pushing down on a piston such that the ratio $L_M/D_M \approx 2$. However, this ratio was not carefully controlled and we estimate that variations of $\pm 15\,\%$ were common. We also had no consistent control over the shape of the piston displacement–time curve. In most cases the initial Re of the vortex that evolved was $\sim 2{\cdot}0 \times 10^4$.

The ring motion was observed by a 35 mm motor-driven framing camera mounted on a 'dolly' that was pushed along, manually, so as to keep the ring image always in the centre of the film frame. On the back of the tank there was an illuminated translucent screen on which were marked the distances from the orifice plate, while a stop-watch in the field of view of the camera gave a time reference.

3.3. *Results and discussion*

In figure 25 we show growth-rate curves that indicate some of the interesting results we have found. The leftmost curve is consistent with the results of Arnold (1974), with a growth rate initially somewhat smaller than that measured by him and then undergoing a transition to a larger value at a later time. The two right-hand curves clearly show a completely different behaviour, undergoing a transition from a relatively large growth rate to one considerably smaller. In terms of concepts we have already introduced we should say that the core flow has become better organized and entrainment into the core has been reduced. Close scrutiny of the photographs shows no obvious difference between rings that grow faster and those that grow slower. The differences are subtle and can probably be unravelled only by detailed observations of mean velocity and turbulence within the ring and ambient fluid. The observation of a reduced growth rate is particularly exciting because it suggests the possibility that the core undergoes a type of transition that is completely different from any we have seen before and opens the way to the discovery of more unexpected mechanisms in the future. We also note that processes introduced in Maxworthy (1974) and summarized in figure 1 (*e*) were clearly in evidence in these experiments. In particular the mixing of ambient fluid into the dyed 'outer-flow region' and the deposition of this mixture into a wake were reconfirmed and serve to strengthen our belief in the basic correctness of this picture.

4. Experiments at the University of Southern California, Los Angeles

4.1. *Introduction*

The motivation for this series of short experiments was a desire to understand the role of certain key features of our model by introducing controlled perturbations into the system. In particular, we were interested in the role played by the core/outer-flow interface and the axial flow introduced by the travelling solitary wave. Three different sets of experiments were performed in a long vertical tank similar to that described in Maxworthy (1974). In the first the ambient fluid was stably stratified, in the second solid objects were introduced into the core to interfere with the axial wave and in the third turbulence was introduced into the ambient fluid. All gave further clues about the ring structure.

4.2. *Apparatus*

The basic apparatus was a vertical tank, 2 m long and of 0·5 m square cross-section. Rings were produced at a sharp-edged orifice 3·8 cm in diameter. In figure 26 we show the three modifications used in this series of experiments: in figure 26 (*a*) a stratified ambient fluid produced by the method introduced by Oster (1965); in figure 26 (*b*) passage of a ring over a thin metal plate that prevented axial core flow, and in figure 26 (*c*) a towed grid to produce ambient turbulence.

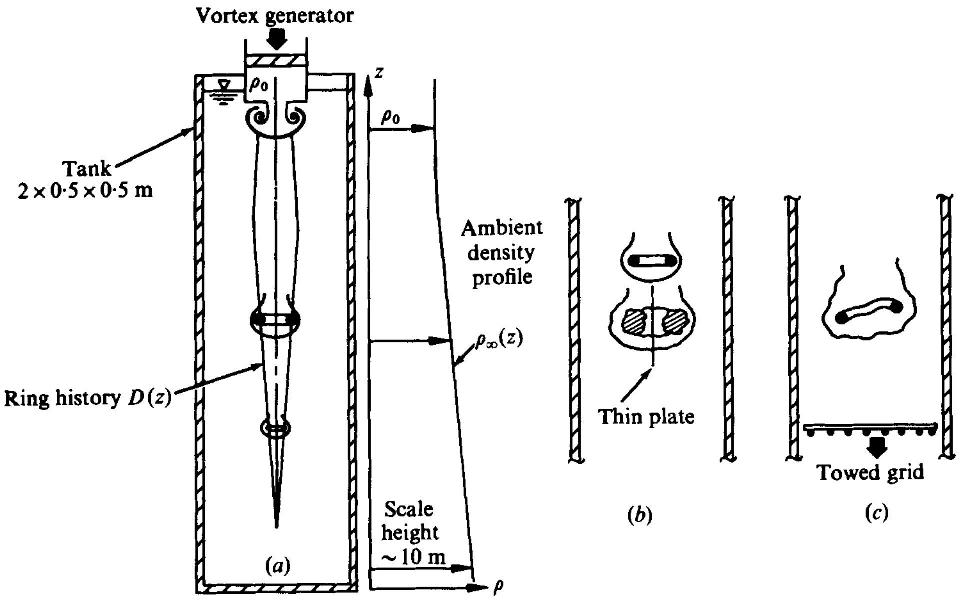

FIGURE 26. Apparatus at U.S.C. (*a*) Ring propagation in a stratified environment. (*b*) Ring passage over a solid object. (*c*) Ring passage through ambient turbulence produced by a towed grid.

In all cases we observed the motion of an initially dyed volume of ejected fluid using a 16 mm movie or a 35 mm framing camera manually towed at the same speed as the vortex ring.

4.3. *Effect of a stratified environment*

In the present experiments a ring was initially formed with a density ρ_0 of $1{\cdot}00\,\mathrm{g/cm^3}$ at the top of the tank. It was then allowed to propagate within an environment of the same density until a 'turbulent' ring had formed (after approximately 50 cm). It then entered a region in which the density increased downwards linearly from 1·00 to $1{\cdot}15\,\mathrm{g/cm^3}$ at the bottom of the tank. The scale height of the density distribution, i.e. $\rho_0\,\partial z/\partial\rho$, was approximately 10 m, i.e. very large compared with the ring diameter. This experiment was first performed mainly out of curiosity, since the theoretical efforts predicted a variety of possible results. Our observation agreed with none of the theories, but when properly interpreted confirmed the basic features of the model presented in Maxworthy (1974) and figure 1(*e*) (and the associated discussion). We have anticipated the result in figure 26(*a*) and show a sequence of photographs in figure 27 (plate 8). After a short distance of growth, the ring's diameter begins to decrease and it is eventually destroyed. In the initial stages of shrinkage the ratio d/D stays approximately constant (i.e. the flow is similar) and the core cross-section is approximately circular, but this ratio increases in the later stages and the core becomes much more distorted. During the whole process the ring velocity decreases monotonically but in the last stages the ring collapse and velocity decrease to zero are quite catastrophic. We note that this decrease in diameter is a consequence of pieces of the core being torn away and mixing into the outer flow and wake. The core responds to the decrease in its volume, initially at least, by maintaining a constant d/D. (One other possibility would have been for D to remain approximately constant and for d to

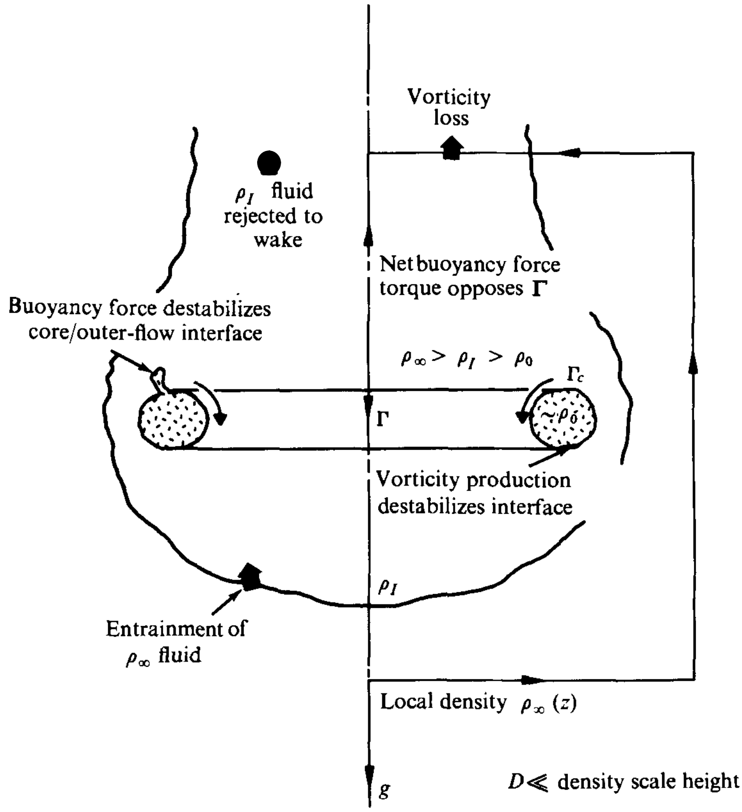

FIGURE 28. Propagation of a 'turbulent' ring through a stratified environment, showing mixing of ambient fluid (ρ_∞) into the outer-flow region to produce fluid of intermediate density (ρ_I). Core fluid still has essentially the same density as initially (ρ_0). Vorticity is produced, baroclinically, because of both the $\rho_I - \rho_\infty$ and the $\rho_0 - \rho_I$ density difference.

decrease alone.) Most of these observations can be simply explained by our model and again point to the fundamental importance of the core/outer-flow interface. In figure 28 we sketch details of this explanation; at the stage shown the ring is well within the stratified part of the tank. Initially the whole moving fluid volume is of density ρ_0; however as it enters the denser fluid the latter mixes across the outer-flow/ambient interface to produce a density intermediate between ρ_0 and local ρ_∞. As the ring propagates further its density ρ_I increases but can never equal ρ_∞. It is this fluid of intermediate density ρ_I that is rejected to the wake. The core has been in contact with this fluid but, because of the very slow entrainment across its interface, it still has a density very close to ρ_0. As a result we arrive at a situation in which three regions of different density are in contact with one another. What is more interesting, however, is what is happening to the vorticity in the system. By considering the net buoyancy torque on the large circuit shown on the right-hand side of figure 28 one can see that the effect of the buoyancy torque due to the difference in density between the outer flow ρ_I and the ambient fluid ρ_∞ is to reduce the total ring circulation. One possibility is that the negative vorticity thus produced diffuses turbulently until it comes in contact with the core interface, where it cancels the core vorticity. This results in a destabilization of the outer skin of the interface, since its mean vorticity is now zero, and it is shed into the outer-flow region and eventually into the wake. However much of the vorticity produced by the difference $\rho_\infty - \rho_I$ must be rejected directly to the wake before it has time to affect the core† and we must appeal to direct baroclinic vorticity production at the core interface itself to explain our results. Since the core is of finite diameter it cannot be perfectly circular and so by considering a circuit around the core itself (figure 28) we see that this results in net vorticity production that opposes the vorticity already in the core.‡ Clearly this is a much more effective way of removing core vorticity and since it can happen only in regions where there are density gradients, i.e. at the interface, the effect is to destabilize this outer layer, which is removed, exposing more of the core, which is in turn destabilized and removed. In the later stages of ring decay, as d/D becomes much larger, eventually approaching unity,§ the buoyancy torque on the core becomes so overwhelming that the final collapse occurs within one or two ring diameters in a fashion reminiscent of Linden's (1973) observations of rings interacting with a sharp density gradient. In this way the circulation of the core is directly reduced and the ring decelerates because the effect of the circulation loss is stronger than that trying to accelerate the ring because of the reduction in its diameter D.||

Unfortunately we cannot explain why the ring stays similar during much of this process as it does, also, in a homogeneous fluid when D is increasing.

We have also extended the calculation of the ring dynamics described in Maxworthy (1974) by allowing for entrainment and detrainment rates that depend on the local Richardson number (i.e. the ratio of buoyancy to inertia forces), and can predict the ring motion during the similarity phase. However, the catastrophic end to the ring's life is not predicted by such a simple model. Clearly, the present paper is not the appropriate place for a detailed discussion, which we leave to a later paper.

4.4. *Changes induced in the core by other external means*

The results of the two final experiments are somewhat harder to interpret unambiguously but nevertheless are of interest. When one allows a ring to propagate over an obstacle (in our case a thin plate aligned with the direction of propagation) the ring structure changes dramatically. One half of the cut ring appears to explode and becomes a diffuse mass of dye while the other undergoes a less dramatic but also rapid change. In figure 29 (*a*) (plate 9) we show photographs of this sequence of events. In only one case out of about twenty did the ring break symmetrically but in all cases the coherence of the core was rapidly destroyed and it became indistinguishable from the

† Observations show that the wake flow immediately behind the ring consists of a strong jet in the opposite direction to the ring motion.

‡ Alternatively, but less satisfyingly, one can think of the core as being convectively unstable.

§ The density difference is also becoming much larger as the ring propagates into denser and denser fluid, because ρ_I increases but the core density stays the same (ρ_0).

|| Cf. the vorticity arguments of Scorer & Davenport (1970) and Crow (1974), in which the baroclinically produced vorticity does not mix into the ring interior but forms a sheath on the outer boundary of the moving fluid volume. This vorticity induces a flow which reduces the vortex ring's diameter D, under which circumstances it accelerates because its circulation is unaltered! In the real case the existence of mixing across the outer-flow/ambient interface is crucial and points to the inadequacy of the theoretical models, which consider only vorticity concentrated into isolated cores.

outer-flow region. We suggest that part of this loss in ring organization is due to the suppression of the axial flow by the obstacle. When such an axial flow is stopped the information about the stoppage travels along the core as a particularly violent vortex jump (or bore). Granger (1968) has shown this most clearly for a bathtub type of vortex. Associated with the wave is an explosive increase in core diameter and decrease in mean vorticity. In terms that we have already introduced the fat core is now very disorganized and grows very rapidly. Since there seems to be only one dominant wave on the core it must get trapped mainly on one side of the obstacle or the other, accounting for the asymmetry in the process. The other side decays more slowly (i) because its stabilizing axial flow has been lost, (ii) because a part of the axial flow might have been stopped by the wall, if the obstacle cut the ring as the wave was passing the edge of the obstacle, and (iii) because of Ekman-layer pumping of fluid into the core at the obstacle.

Finally we looked at the effect of introducing grid turbulence upstream of the moving ring. Several qualitative observations are of interest and these can be interpreted in terms of our model. For the grid spacing of these experiments (a 5×5 cm square array of 1 cm diameter rods) the upstream turbulence is mainly of a scale comparable to the ring diameter. The main difference is that the turbulence has vorticity of random sign whereas in the ring it is predominantly of one sign. The turbulent fluid penetrates into the outer-flow region, mixes with the fluid there and comes into intimate contact with the core. This results in an increased fluctuation level at the core/outer-fluid interface and enhanced entrainment. Occasionally, especially if the ring is allowed to follow closely behind the grid, the vorticity levels are so high that they are capable of completely cancelling a large segment of core vorticity and the coherence of the core is completely destroyed (cf. the obstacle experiments). At lower levels, i.e. further behind the grid, the core becomes distorted, stretched and thinned before it eventually disintegrates (figure 29*b*) and its growth occurs in discontinuous jumps rather than smoothly, as in Arnold (1974).

5. Conclusions: discussion of core 'organization'

Many of the comments that would normally pass as conclusions are contained in the summary material of § 1, and it seems unnecessary to repeat them here. However, one concept has arisen in the later part of this paper that does deserve further discussion: that of ring 'organization'. As used, for example, in § 2.2.4 (*d*) its qualitative meaning is clear: well-organized rings having well-defined core/outer-flow interfaces and, especially, low growth rates α. In fact α is probably the best quantitative indicator of the degree of organization, being a gross parameter that includes all possible effects that could cause a change in ring structure. In the interest of trying to unravel the various ingredients that could eventually give a particular value of α, we have also looked at a variety of other possible parameters. Several arguments have validity. Since, as we have stated, the organization is controlled by the core structure its ability to withstand interaction with the turbulence in the outer-flow region is one possible measure. We can compare the maximum core velocity $\sim \Gamma/d$ with the typical outer-flow velocity U_T to obtain $\Gamma/U_T d$ as one possibility. Comparing the core vorticity Γ/d^2 with the outer-flow vorticity, either U_T/D or Γ/D^2, gives either $(\Gamma/U_T d)\, D/d$ or D/d. We have taken both the present data and those of Sallet & Widmeyer (1974) and Liess & Didden (1975*b*) and tried to assess the validity of the above dimensionless quantities. For example, the 'laminar' rings of Sallet & Widmeyer (1974) have $\alpha \approx 1{\cdot}5\times10^{-5}$ while their 'turbulent 'rings have $\alpha \approx 5\times10^{-3}$. Of all the parameters mentioned none shows a clear trend although $\Gamma/U_T d$ does tend to be somewhat higher ($\sim 15\%$) for the 'laminar' rings. The data of Liess & Didden (1975*b*), and our own, show that at least in the flow before instability all the above-mentioned parameters increase rapidly as $\overline{Re}_M$ increases. There are clear differences only between our data for high $\overline{Re}_M$ and those of Liess & Didden (1975, 1976), for low $\overline{Re}_M$, in that our values of α are much smaller and all of the above-mentioned parameters much larger. However within our own data (table 1) there is no clear trend with $\overline{Re}_M$ as we might expect. We suspect that the differences are due to slight changes in conditions from run to run, e.g. changes in the pattern of wave breaking, interaction with a small amount of ambient turbulence, the appearance of other possible types of core waves (e.g. sinuous modes) etc., that somehow change the entrainment rate at the core/outer-flow interface. At the moment only α is a good measure of this process; any other quantity seems to be of little proven value.

The effort of getting this work to the manuscript stage has taken place in so many different locations that in trying to thank all those involved this section could double the length of the paper! At M.P.I.S., Dr Christian Liess and Dipl.Phys. Norbert Didden were generous with their time and talents far beyond the normal limits of hospitality. They helped familiarize me with the apparatus, provided all supporting services and above all listened to, commented upon and added to the ideas presented here. Cand.phys. Hans-Heinrich Claus was given the unenviable task of reducing much of the photographic data, which he did with dispatch, accuracy and unfailing good nature. I also wish to thank Prof. E. A. Müller for giving me the opportunity to visit Göttingen and for so generously providing such salubrious surroundings. At Caltech, Prof. Fred Raichlen most graciously allowed the use of a vital piece of apparatus between the times it was being used by his graduate students; while discussions with Prof. P. G. Saffman and Dr V. Kulkarny added immeasurably to my understanding of the experimental results. At U.S.C., Casey De Vries and Herbert Lloyd designed and constructed most of the apparatus while many students helped with the experiments. This paper was written while I was an Advanced Study Program Senior Postdoctoral Fellow at the National Center for Atmospheric Research, an organization sponsored by the National Science Foundation. I should like to thank the many people there who made my stay such a pleasant one and provided so much essential help and support. Finally, much of the experimental work and my effort was supported by the N.S.F. through Grant GK-38147X to the University of Southern California.

Appendix. A simple model of the ring formation process

We assume that the fluid forming the core is that which has gained vorticity from viscous diffusion processes at the lip. The model relates only the mass balance between the initial boundary layers and the final ring and says nothing about the dynamics of the process (i.e. how much vorticity is formed).

For an ejected slug of length L_M and velocity $\overline{U}_M$ the main viscous layer has a thickness $(\nu L_M/K_1\overline{U}_M)^{\frac{1}{2}}$ (figure 17). The induced layer of negative vorticity has a thickness $\{\nu L_M/K_2\overline{U}_M\}^{\frac{1}{2}}$. Here $K_1(\overline{Re}_M)$ and $K_2(\overline{Re}_M)$ attempt to represent the fact that the velocities depend somehow on the rolling-up process, which in turn is dependent on $\overline{Re}_M$. Thus the total volume of vortical fluid is

$$\sim \left[\left\{\frac{\nu L_M}{\overline{U}_M}\right\}^{\frac{1}{2}} \left\{\frac{1}{K_1^{\frac{1}{2}}}+\frac{1}{K_2^{\frac{1}{2}}}\right\}\right] D_M L_M$$

We assume that this rolls up to form a core with a vorticity distribution that is similar at all values of $\overline{Re}_M$ and has a diameter d, with a ring diameter D and ring volume $\sim d^2D$.

Equating these we obtain an expression for d and then by assuming that

$$\lambda = \text{constant} \times d = \pi D/n$$

we obtain
$$n \sim \overline{Re}_M^{\frac{1}{4}} \left(\frac{D}{D_M}\right)^{\frac{3}{2}} \left(\frac{D_M}{L_M}\right)^{\frac{3}{4}} \left(\frac{1}{K_1^{\frac{1}{2}}}+\frac{1}{K_2^{\frac{1}{2}}}\right)^{-\frac{1}{2}}.$$

We further assume, as suggested by figure 8 and the associated discussion, that

$$\frac{D}{D_M} \sim \left(\frac{L_M}{D_M}\right)^p \overline{Re}_M^q,$$

in which case
$$n \sim \overline{Re}_M^{\frac{1}{4}(1+6q)} \left(\frac{L_M}{D_M}\right)^{\frac{3}{4}(2p-1)} \left(\frac{1}{K_1^{\frac{1}{2}}}+\frac{1}{K_2^{\frac{1}{2}}}\right)^{-\frac{1}{2}}.$$

From figure 8 we have already noted that $p \approx \frac{1}{4}$ or $n \sim (L_M/D_M)^{-\frac{3}{8}}$. This result is consistent with the observations that n decreases as L_M/D_M increases and that the dependence is weak.

In its simplest form the Reynolds number dependence is given by $\overline{Re}_M^{\frac{1}{4}}$. Even if we ignore the effects of K_1 and K_2 the weak $\overline{Re}_M$ dependence of L_M/D_M (figure 8) can increase the exponent to a value around 0·3. Unfortunately the data of figure 9 give only an idea of the $\overline{Re}_M$ dependence of $K_1 - K_2$ and not each independently, but we anticipate that these too will tend to increase the value of exponent quoted above. For further comments see §2.2.3.

REFERENCES

Arnold, O. 1974 Verhalten von Wirbelringen in turbulenzarmer und turbulenter Umgebung. Ph.D. dissertation, University of Karlsruhe, W. Germany.

Betz, A. 1932 *N.A.C.A. Tech. Memo* no. 713.

Crow, S. C. 1974 The motion of a vortex pair in a stratified fluid. *Poseidon Res. Corp. Rep.* no. 1.

Granger, R. A. 1968 Speed of a surge in a bathtub vortex. *J. Fluid Mech.* **34**, 651–656.

Krutzsch, C.-H. 1939 Über eine experimentelle beobachtete Erscheinung an Wirbelringen bei ihrer translatorischen Bewegung in wirklicher Flüssigkeit. *Ann. Phys.* **35**, 497–523.

Kulkarny, V. A. 1977 On vortex formation near sharp edges in impulsive flows. Submitted to *J. Fluid Mech.*

Lamb, H. 1932 *Hydrodynamics*, p. 241. Dover.

Leibovich, S. & Randall, J. D. 1972 Solitary waves in concentrated vortices. *J. Fluid Mech.* **51**, 625–635.

Liess, C. & Didden, N. 1975 Experimentelle Untersuchung von Ringwirbeln. 50 *Jahre M. P. I. Strömungsforschung, Göttingen.*

Liess, C. & Didden, N. 1976 Experimente zum Einfluss der Anfangsbedingungen auf die Instabilität von Ringwirbeln. *Z. angew. Math. Mech.* **56**, T206–T208.

LINDEN, P. F. 1973 The interaction of a vortex ring with a sharp density interface: a model for turbulent entrainment. *J. Fluid Mech.* **60**, 467–480.

MAXWORTHY, T. 1972 The structure and stability of vortex rings. *J. Fluid Mech.* **51**, 15–32.

MAXWORTHY, T. 1974 Turbulent vortex rings. *J. Fluid Mech.* **64**, 227–239.

MOORE, D. W. 1974 A numerical study of the roll-up of a finite vortex sheet. *J. Fluid Mech.* **63**, 225–235.

MOORE, D. W. & SAFFMAN, P. G. 1973 Axial flow in laminar trailing vortices. *Proc. Roy. Soc.* A **333**, 491–508.

MOORE, D. W. & SAFFMAN, P. G. 1975 The instability of a straight vortex filament in a strain field. *Proc. Roy. Soc.* A **346**, 413–425.

OSTER, G. 1965 Density gradients. *Sci. Am.* **213** (2), 70–76.

PRANDTL, L. 1961 *Gesammelte Abhandlungen zur angewandten Mechanik, Hydro- und Aerodynamik*, 2nd edn, pp. 697–713. Springer.

SAFFMAN, P. G. 1976 On the formation of vortex rings. *Stud. Appl. Math.* **51**, 261–268.

SALLET, R. S. & WIDMEYER, D. W. 1974 An experimental investigation of laminar and turbulent vortex rings in air. *Z. Flugwiss.* **22**, 207–215.

SCORER, R. S. & DAVENPORT, L. J. 1970 Contrails and aircraft downwash. *J. Fluid Mech.* **43**, 451–464.

WIDNALL, S. E., BLISS, D. B. & TSAI, C. Y. 1974 The instability of short waves on a vortex ring. *J. Fluid Mech.* **66**, 35–47.

WIDNALL, S. E. & SULLIVAN, J. P. 1973 On the stability of vortex rings. *Proc. Roy. Soc.* A **332**, 335–353.

YUEN, H. C. 1973 Waves on vortex filaments. Ph.D. dissertation, California Institute of Technology.

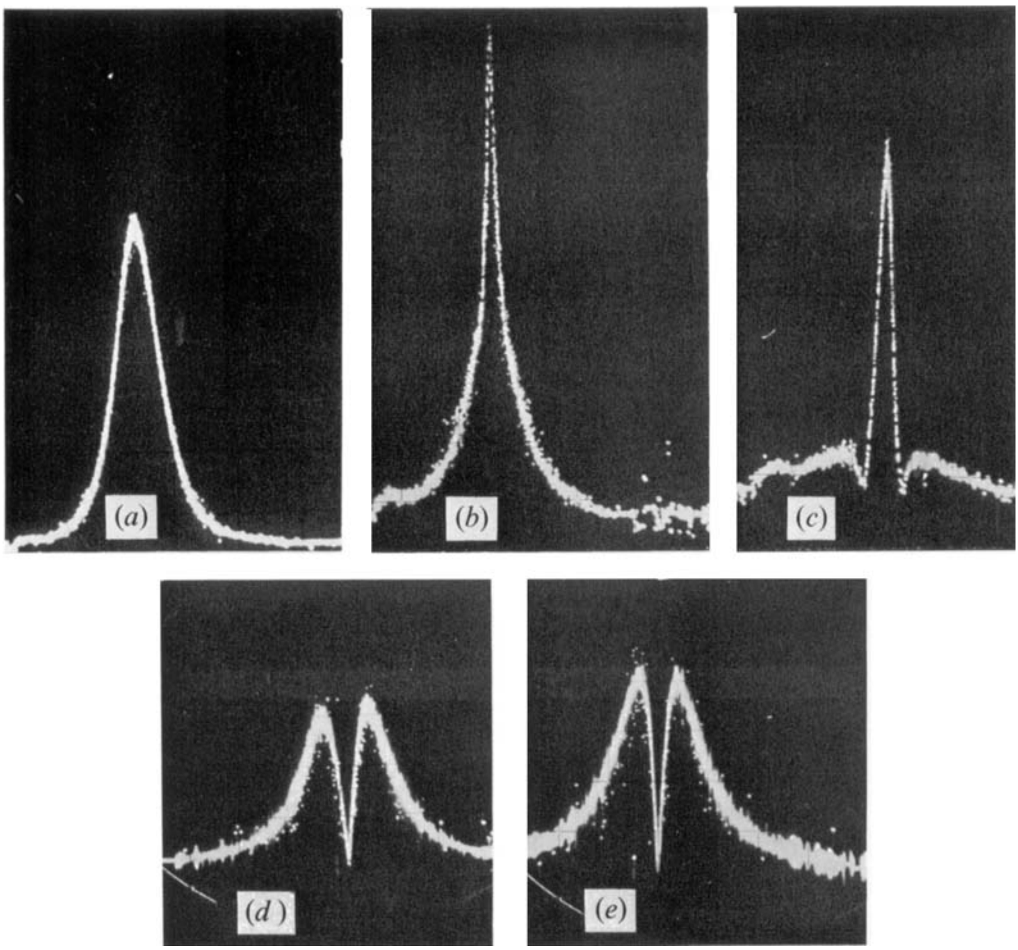

FIGURE 3. $U(x)$ and $V(x)$ traverses through a vortex ring at various levels corresponding to the velocity profile shown in figure 4. The thickness of the trace is an indication of the instrument noise level, since the flow is laminar in this case. U component: (*a*) $r = 0$, (*b*) $r = 3{\cdot}375$ cm, (*c*) $r = 4{\cdot}5$ cm. V component: (*d*) $r = 1{\cdot}5$ cm, (*e*) $r = 4{\cdot}5$ cm. All with calibration $5{\cdot}71$ kHz (cm/s)$^{-1}$, $0{\cdot}01$ V kHz^{-1} and $0{\cdot}2$ V cm^{-1}. Sweeps at (*a*)–(*c*) $0{\cdot}2$ s cm^{-1} and (*d*), (*e*) $0{\cdot}1$ s cm^{-1}.

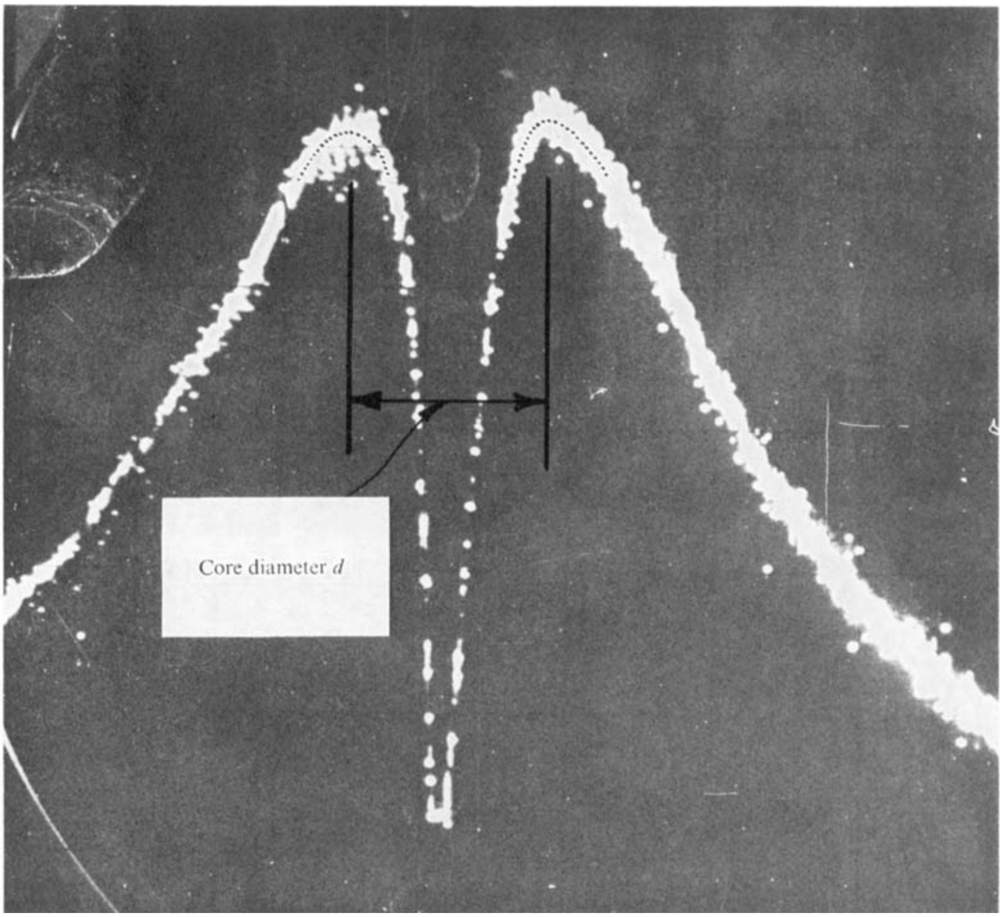

FIGURE 5. LDV output showing $V(x)$ at the level $r = R$, i.e. through centre of vorticity concentration. Showing definition of core diameter d. Owing to the directional ambiguity of the LDV system all velocities appear positive even though those to the right of the line of symmetry are, in fact, negative. $[U_T D/\nu = 2{\cdot}1 \times 10^4.]$

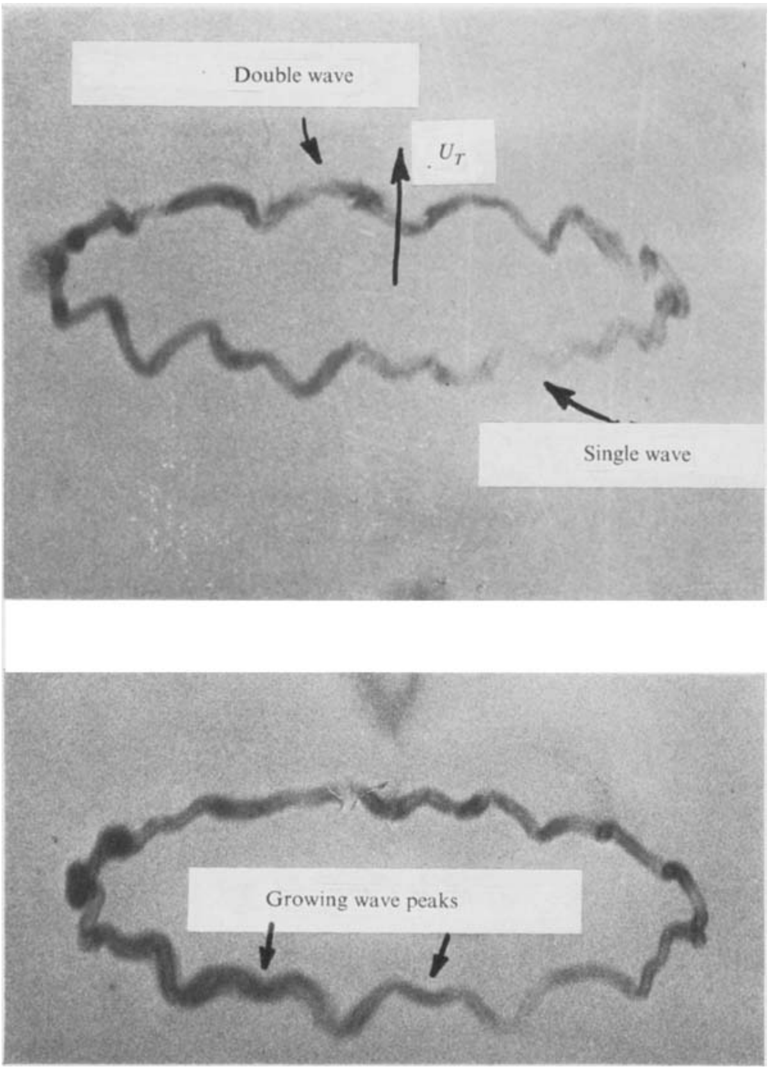

FIGURE 13. Photograph showing the form taken by the instability. Note that waves of one wavelength and ones with exactly twice that wavelength exist on the core at the same time. $\overline{Re}_M = 4{\cdot}5 \times 10^4$, $L_M/D_M = 2{\cdot}0$.

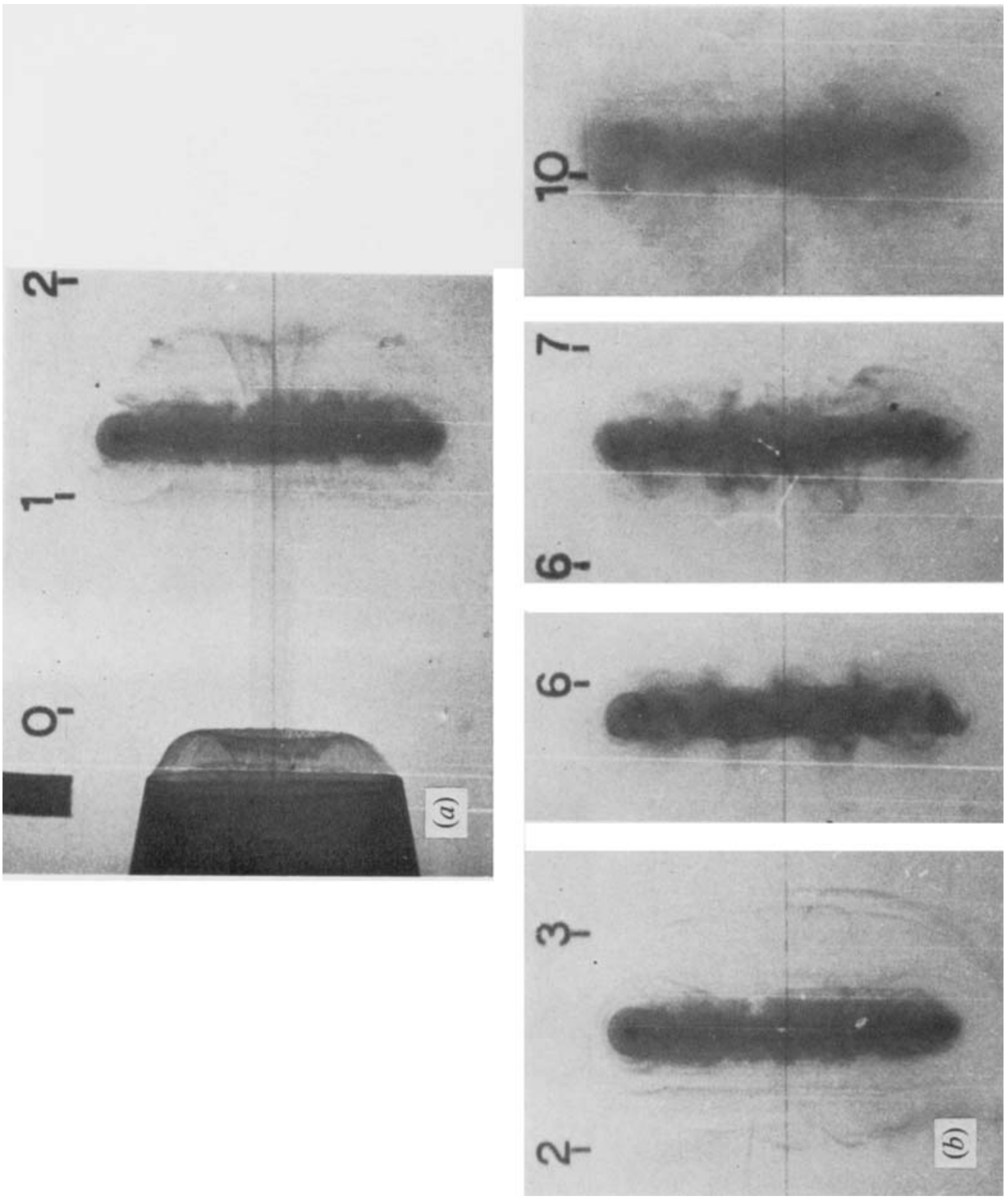

FIGURE 16. (*a*) Photograph from 16 mm moving-picture sequence showing secondary vortex production at low $\overline{Re_M}$ (as in figure 15*a*). (*b*) Wave breaking in the same ring to form a disorganized vortex core. Numbers on the background indicate distance from the nozzle exit in decimetres.

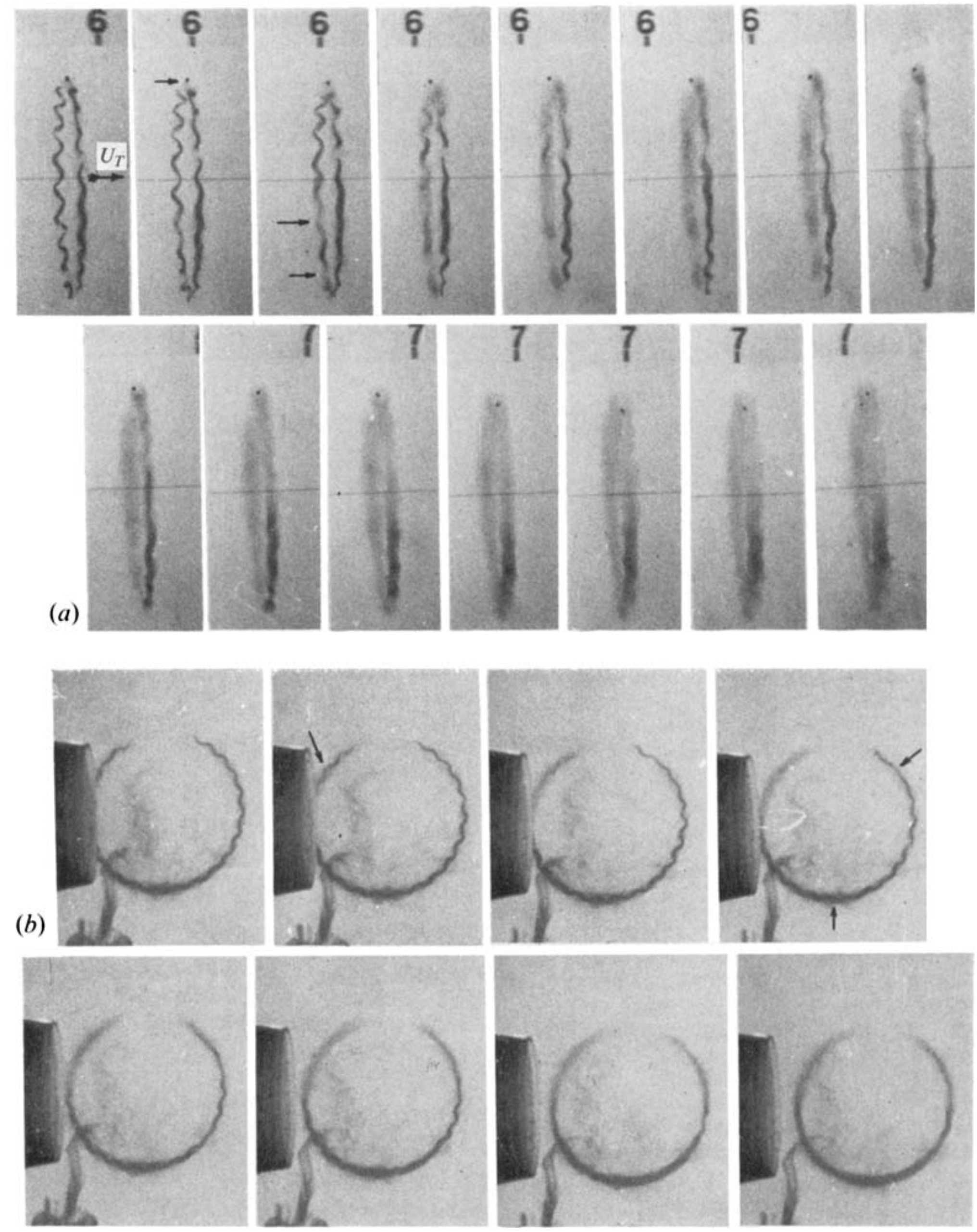

FIGURE 18. Photographs from moving-picture sequence showing breaking of finite amplitude waves at high $\overline{Re}_M$. Note preferential breaking of waves at locations indicated by the arrows. Non-uniformity in the dye line is due to blockage of parts of the dye injection slot by algae. (*a*) Side view. Also note motion of a small bubble at the top of the ring in the axial flow produced by the wave ($\overline{Re}_M \sim 4{\cdot}6 \times 10^4$). (*b*) Plan view taken by using the 45° mirror shown in figure 2 ($\overline{Re}_M \sim 7{\cdot}4 \times 10^4$). Pictures are taken 0·03 s apart. Numbers are distance from nozzle in decimetres.

MAXWORTHY

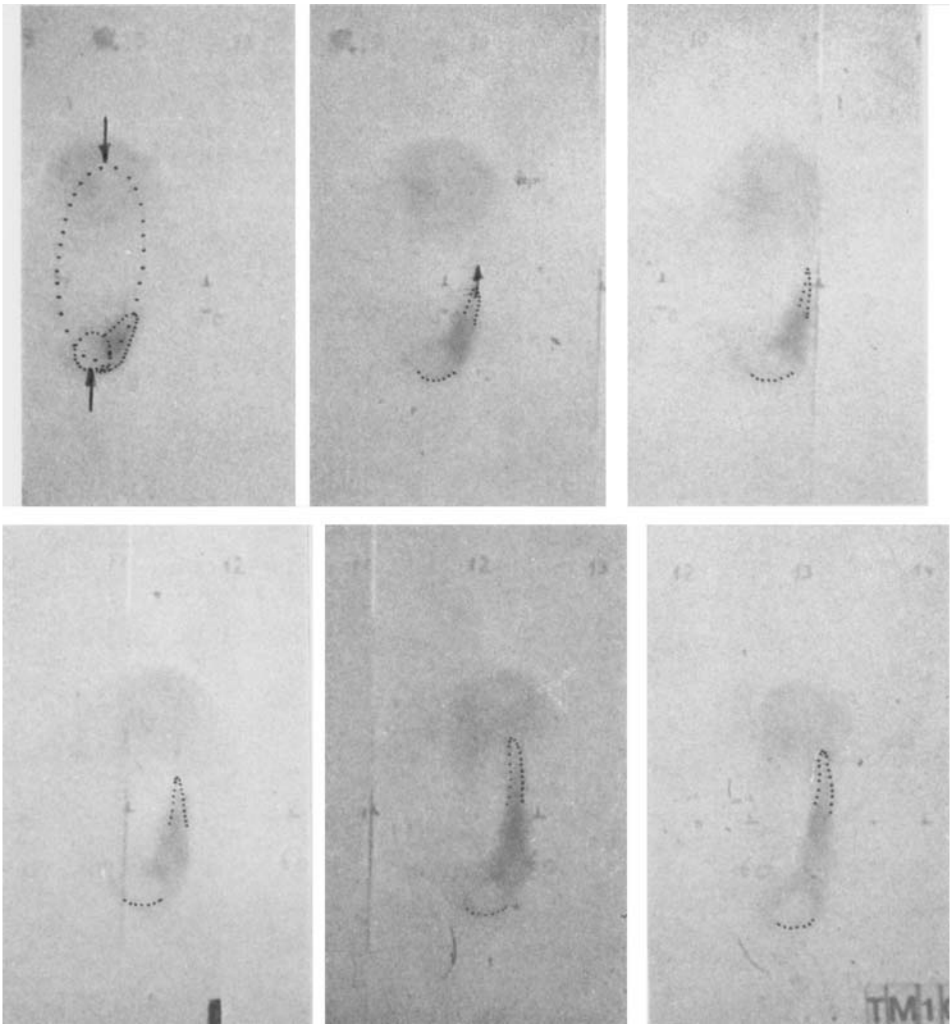

FIGURE 19. Sequence from moving-picture film of axial flow in core. Photographed from a location ahead and to the side of the ring, so that it appears elliptical in these photographs (shown dotted in the first photograph). Dye that now spreads around core started at top and bottom of ring, as indicated by the arrows. Because of the poor photographic reproduction we have dotted in the locations of the bottom of the ring and the tip of the displaced dye. Pictures are 0·12 s apart.

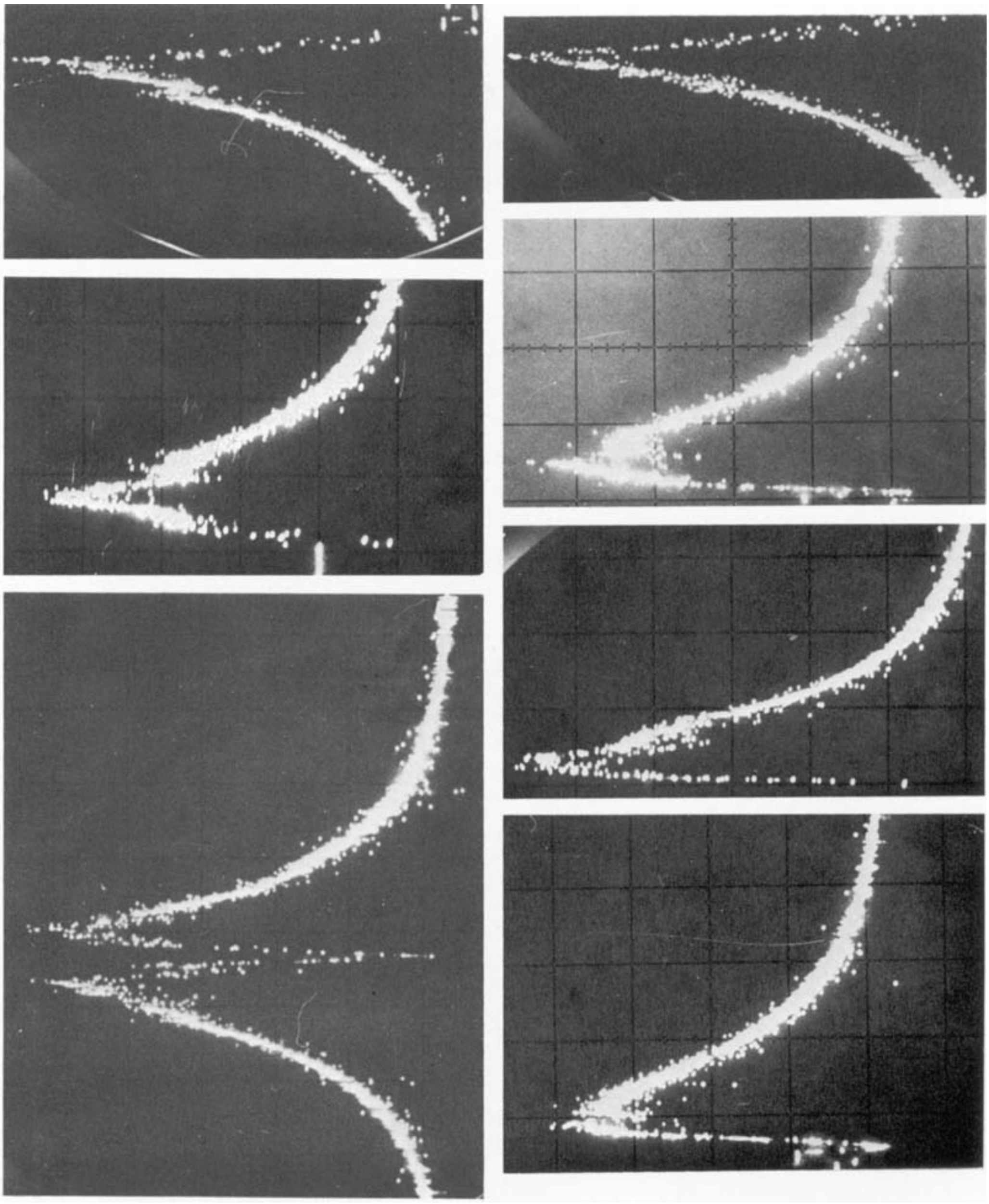

FIGURE 20. V velocity traces through turbulent vortex cores at $14D_M$. For a variety of cases.

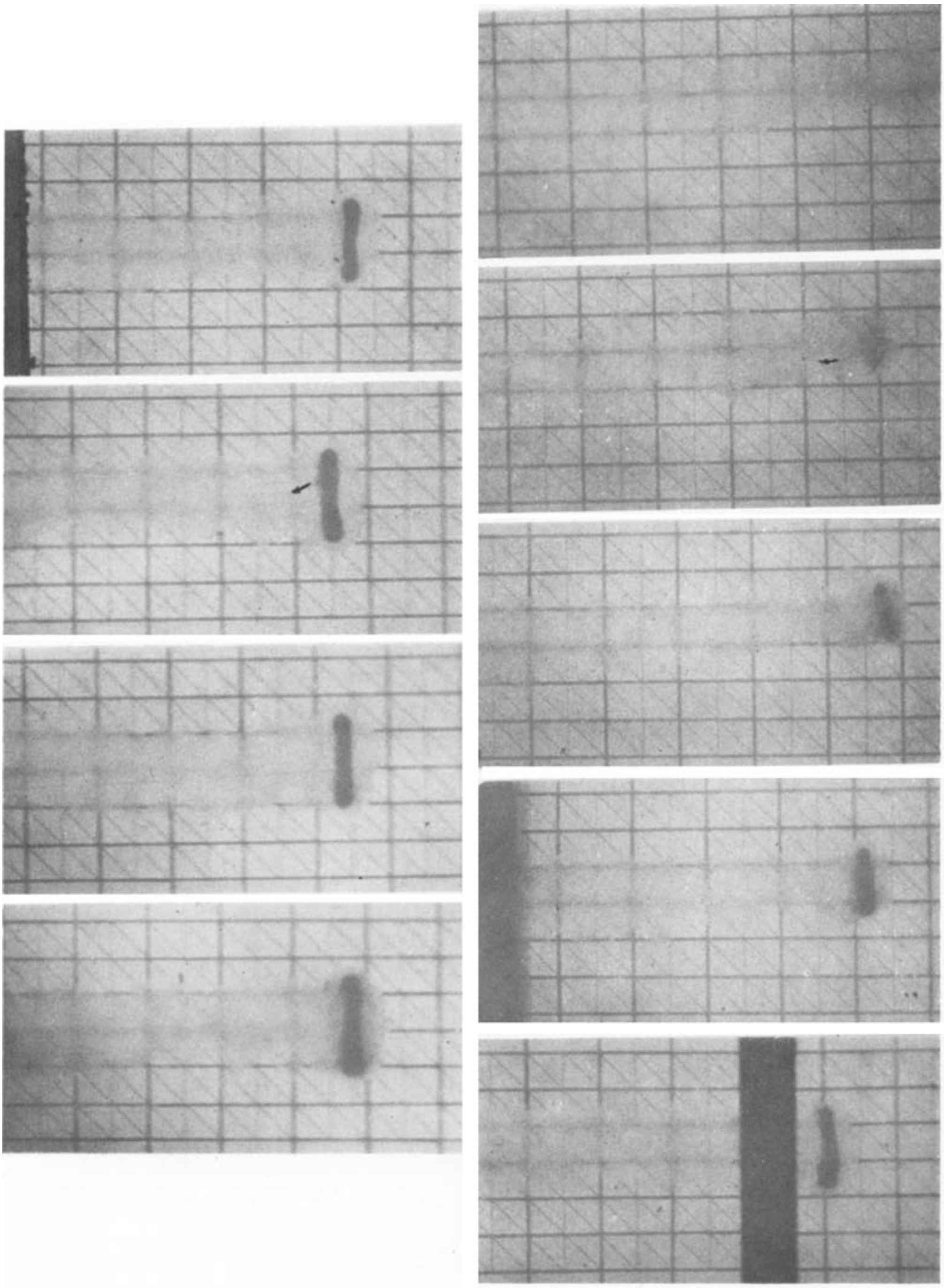

FIGURE 27. Photographs taken from a moving-picture sequence of a vortex ring propagating through a stratified environment. Note loss of dyed core material and decrease in ring diameter D, and the mixing and dye loss to the wake! Note also the clearly defined interfaces between all three regions of different density. The ultimate flow after the ring had disappeared consisted of the whole wake region oscillating vertically at the intrinsic frequency of the basic stratification, i.e. $[g/\rho_0\, \partial\rho/\partial z]^{\frac{1}{2}}$.

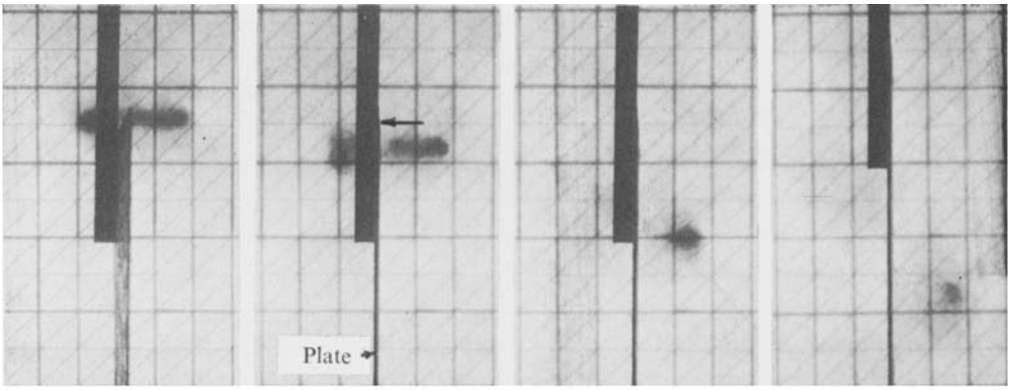

(a)

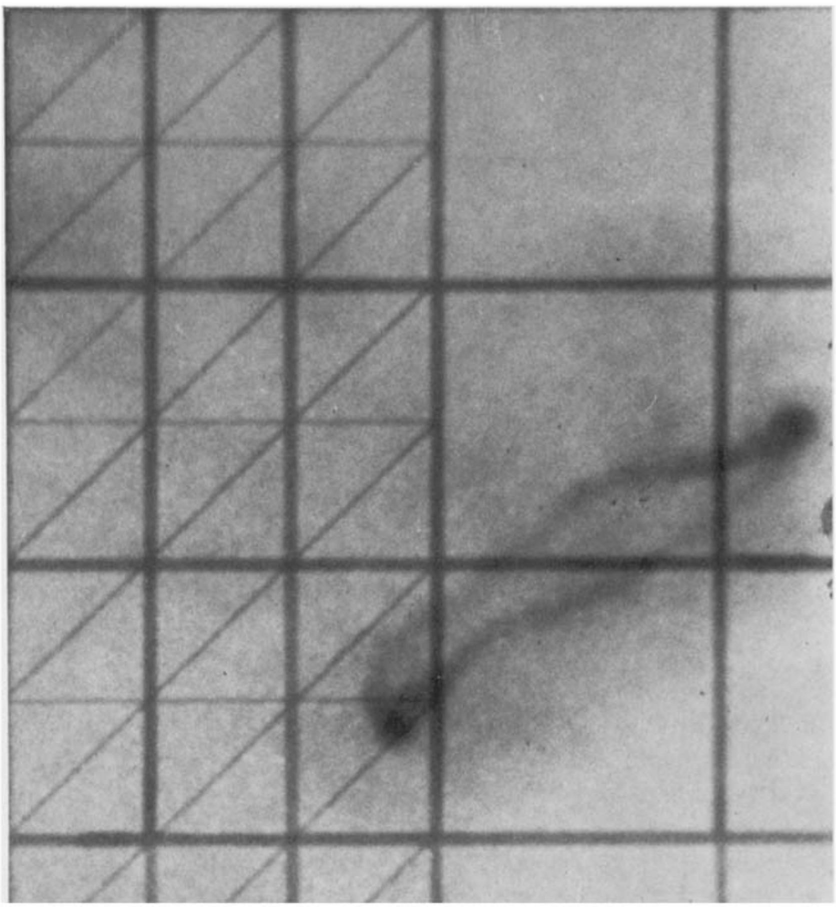

(b)

FIGURE 29. (*a*) Motion of a vortex ring over a thin plate aligned with the direction of propagation. Note asymmetry of response and almost complete destruction of the left-hand side of the ring. Arrow in second photo indicates the top edge of the plate. (*b*) One effect of upstream turbulence on a vortex ring. Note stretching and thinning of vortex core (which at this station would have looked like the initial ring in (*a*), if there had been no turbulence in the ambient fluid).